Water-stable isotopes in the LMDZ4 general circulation model: Model evaluation for present-day and past climates and applications to climatic interpretations of tropical isotopic records

Camille Risi, Sandrine Bony, Françoise Vimeux, Jean Jouzel

▶ **To cite this version:**

Camille Risi, Sandrine Bony, Françoise Vimeux, Jean Jouzel. Water-stable isotopes in the LMDZ4 general circulation model: Model evaluation for present-day and past climates and applications to climatic interpretations of tropical isotopic records. Journal of Geophysical Research: Atmospheres, 2010, 115 (D12), pp.D12118. 10.1029/2009jd013255 . hal-01142300

HAL Id: hal-01142300
https://hal.science/hal-01142300

Submitted on 15 Apr 2015

HAL is a multi-disciplinary open access archive for the deposit and dissemination of scientific research documents, whether they are published or not. The documents may come from teaching and research institutions in France or abroad, or from public or private research centers.

L'archive ouverte pluridisciplinaire **HAL**, est destinée au dépôt et à la diffusion de documents scientifiques de niveau recherche, publiés ou non, émanant des établissements d'enseignement et de recherche français ou étrangers, des laboratoires publics ou privés.

JOURNAL OF GEOPHYSICAL RESEARCH, VOL. 115, D12118, doi:10.1029/2009JD013255, 2010

Click Here for Full Article

Water-stable isotopes in the LMDZ4 general circulation model: Model evaluation for present-day and past climates and applications to climatic interpretations of tropical isotopic records

Camille Risi,[1] Sandrine Bony,[1] Françoise Vimeux,[2] and Jean Jouzel[3]

Received 27 September 2009; revised 18 December 2009; accepted 13 January 2010; published 23 June 2010.

[1] We present simulations of water-stable isotopes from the LMDZ general circulation model (the LMDZ-iso GCM) and evaluate them at different time scales (synoptic to interannual). LMDZ-iso reproduces reasonably well the spatial and seasonal variations of both $\delta^{18}O$ and deuterium excess. When nudged with reanalyses, LMDZ-iso is able to capture the synoptic variability of isotopes in winter at a midlatitude station, and the interannual variability in mid and high latitudes is strongly improved. The degree of equilibration between the vapor and the precipitation is strongly sensitive to kinetic effects during rain reevaporation, calling for more synchronous vapor and precipitation measurements. We then evaluate the simulations of two past climates: Last Glacial Maximum (21 ka) and Mid-Holocene (6 ka). A particularity of LMDZ-iso compared to other isotopic GCMs is that it simulates a lower d excess during the LGM over most high-latitude regions, consistent with observations. Finally, we use LMDZ-iso to explore the relationship between precipitation and $\delta^{18}O$ in the tropics, and we discuss its paleoclimatic implications. We show that the imprint of uniform temperature changes on tropical $\delta^{18}O$ is weak. Large regional changes in $\delta^{18}O$ can, however, be associated with dynamical changes of precipitation. Using LMDZ as a test bed for reconstructing past precipitation changes through local $\delta^{18}O$ records, we show that past tropical precipitation changes can be well reconstructed qualitatively but not quantitatively. Over continents, nonlocal effects make the local reconstruction even less accurate.

Citation: Risi, C., S. Bony, F. Vimeux, and J. Jouzel (2010), Water-stable isotopes in the LMDZ4 general circulation model: Model evaluation for present-day and past climates and applications to climatic interpretations of tropical isotopic records, *J. Geophys. Res.*, *115*, D12118, doi:10.1029/2009JD013255.

1. Introduction

[2] Because of differences in mass and symmetry of the main isotopic forms of the water molecule ($H_2^{16}O$, HDO, $H_2^{18}O$), an isotopic fractionation occurs during phase changes depending on atmospheric conditions. As a consequence, water-stable isotopes are widely used as a tracer of past climate variations and of the present-day water cycle. In particular, the isotopic composition recorded in polar ice cores have long been used to reconstruct past temperatures [*Dansgaard*, 1953; *Jouzel*, 2003]. More recently, the isotopic composition recorded in low-latitude ice cores [*Thompson et al.*, 2000; *Ramirez et al.*, 2003] or speleothems [*Wang et al.*, 2008; *Cruz et al.*, 2005a] have also been used to infer past temperatures [*Thompson et al.*, 2000] or precipitation rates [*Hoffmann et al.*, 2003].

[3] However, processes that control the water isotopic composition are numerous and complex. For the Greenland ice cores, for example, using the spatial slope as a surrogate for the temporal slope to evaluate past local temperature changes leads to a large uncertainty of a factor of 2 [*Jouzel*, 1999; *Jouzel*, 2003]. This could be due to a change in air mass origins [*Werner et al.*, 2001] or in precipitation seasonality [*Krinner et al.*, 1997b; *Krinner and Werner*, 2003], or to a dampening of isotopic changes by ocean evaporation [*Lee et al.*, 2008]. At low latitudes, the paleoclimatic interpretation of isotopic records is even less quantitative. Most of the tropical precipitation arises from convective processes, which strongly affect the isotopic composition of both vapor and precipitation [*Lawrence et al.*, 2004; *Bony et al.*, 2008; *Risi et al.*, 2008a, 2008b]. While the earliest interpretation of Andean ice cores had linked isotopes to temperatures [*Thompson et al.*, 2000], more recent studies have stressed the importance of the precipitation intensity upstream the air mass trajectories [*Hoffmann*, 2003; *Vimeux et al.*, 2005] and the role of tropical Pacific sea surface temperatures (SSTs) on the isotopic variability in Andean ice core records [*Bradley et al.*, 2003]. As a consequence, while Rayleigh distillation models (representing the loss of

[1] LMD, IPSL, UPMC, CNRS, Paris, France.
[2] UR Great Ice, IRD, LSCE, IPSL, (CEA, CNRS, UVSQ), Gif-sur-Yvette, France.
[3] LSCE, IPSL (CEA, CNRS, UVSQ), Gif-sur-Yvette, France.

Copyright 2010 by the American Geophysical Union.
0148-0227/10/2009JD013255

heavier isotopes during condensation and precipitation) are useful to study at first order the evolution of air masses as they are transported from a moisture source region to higher latitudes [*Ciais and Jouzel*, 1994], more complex models are necessary to take into account the numerous processes affecting the isotopic composition of precipitation.

[4] Atmospheric general circulation models (GCM) are now frequently used for isotopic studies. They represent the three-dimensional transport of air masses and isotopes as well as large-scale condensation and atmospheric convection, albeit in a parameterized way. Since the pioneering work of *Joussaume et al.* [1984], water isotopes have been implemented in at least a half-dozen GCMs: GISS [*Jouzel et al.*, 1987; *Schmidt et al.*, 2007], ECHAM [*Hoffmann et al.*, 1998], MUGCM [*Noone and Simmonds*, 2002a], GENESIS [*Mathieu et al.*, 2002], CAM [*Lee et al.*, 2007], GSM [*Yoshimura et al.*, 2008], Hadley GCM [*Tindall et al.*, 2009] as well as in regional models (REMO [*Sturm et al.*, 2005]). They have been used, for example, to better understand how the climatic signal is recorded by isotopes in ice cores, at the interannual to decadal time scales [*Vuille et al.*, 2003; *Vuille and Werner*, 2005] and at paleoclimatic time scales [*Werner et al.*, 2001].

[5] In this paper, we present the implementation of water-stable isotopes in the LMDZ4 model (whose isotopic version is hereafter named LMDZ-iso). The LMDZ4 model is the GCM developed at the Laboratoire de Mtorologie Dynamique (LMD) [*Hourdin et al.*, 2006]. It is the atmospheric component of the Institut Pierre Simon Laplace (IPSL) ocean-land-atmosphere coupled model [*Marti et al.*, 2005] that participated in CMIP3 [*Meehl et al.*, 2007]. Its dynamical and physical packages have completely changed since the pioneering work of *Joussaume et al.* [1984]. An interesting particularity of this GCM now is the possibility of using stretched grids [*Hourdin et al.*, 2006], allowing studies at both global and regional scales [e.g., *Krinner et al.*, 1997a].

[6] The first goal of this paper is to evaluate the simulation of water-stable isotopes by LMDZ-iso at different time scales. We evaluate the present-day isotopic spatial and seasonal distribution and the isotopic variability at time scales ranging from synoptic to interannual. For this purpose, we have performed an Atmospheric Model Intercomparison Project (AMIP) [*Gates*, 1992] simulation forced by monthly observed SSTs from 1979 to 2007. To evaluate the isotopic simulation in a more rigorous way, we have also performed an AMIP simulation over the same period with the large-scale atmospheric dynamics nudged by meteorological reanalyses. Since a particular effort has been invested in the representation of the droplet reevaporation in the model [*Bony et al.*, 2008], we pay particular attention to evaluating the equilibrium between droplets and water vapor using simultaneous vapor and precipitation data available at some stations. We also pay a lot of attention to evaluating the d excess, which is sensitive to kinetic fractionation notably during rain reevaporation. Finally, we evaluate the isotopic distribution for two past climates for which isotopic data are available: Last Glacial Maximum (21,000 years ago, 21 ka) and Mid-Holocene (6 ka).

[7] The second goal is to use LMDZ-iso to investigate the controls of the isotopic composition of precipitation in the tropics, where the paleoclimatic interpretation is the most uncertain. In particular, what are the relative influences of temperature and precipitation changes on the isotopic composition of tropical precipitation? How useful may $\delta^{18}O$ records be for reconstructing past local precipitation changes in the tropics?

[8] In section 2, we describe the LMDZ4 model, the implementation of water-stable isotopes and the various simulations performed. In section 3, we evaluate the simulation of the isotopic composition for the present-day climatology, synoptic variability, interannual variability and past climates. In section 4, we use LMDZ-iso to explore what paleoclimatic information is recorded in tropical isotopic records. We conclude and give perspectives in section 5.

2. Model and Simulations Description

[9] In this section we briefly describe the LMDZ4 GCM, the implementation of water-stable isotopes and the different simulations performed.

2.1. LMDZ4 GCM

[10] The dynamical equations are discretized in a latitude-longitude grid, with a standard resolution of 2.5° × 3.75° and 19 vertical levels. Water in its vapor and condensed forms is advected by the Van Leer advection scheme [*Van Leer*, 1977], which is a monotonic second-order finite volume scheme. The physical package is described in detail by *Hourdin et al.* [2006]. It includes in particular the Emanuel convective parameterization [*Emanuel*, 1991; *Grandpeix et al.*, 2004] coupled to the *Bony and Emanuel* [2001] cloud scheme. Each grid cell is divided into four subsurfaces: ocean, land, ice sheet and sea ice. In the stand-alone version of LMDZ4 used here, the land surface is represented as a simple bucket model, and land surface evaporation is calculated as a single flux: no distinction is made between transpiration, bare soil evaporation, or evaporation of intercepted water by the canopy.

2.2. Isotopic Processes

[11] Water isotopic species ($H_2^{16}O$, $H_2^{18}O$ and HDO) are transported and mixed passively by the large-scale advection and various air mass fluxes. In the Van Leer advection scheme, it is assumed that the water content advected from one box to the next is a linear combination of the water contents in the two grid boxes involved. For numerical reasons, we assume similarly that the isotopic ratio of the water advected from one box to the next (rather than the isotopic content) is a linear combination of the isotopic ratios in the two grid boxes involved (Appendix A).

[12] Equilibrium fractionation coefficients between vapor and liquid water or ice are calculated after *Merlivat and Nief* [1967] and *Majoube* [1971a, 1971b]. We take into account kinetic effects during the evaporation from the sea surface following *Merlivat and Jouzel* [1979] and during snow formation following *Jouzel and Merlivat* [1984], with the supersaturation parameter λ set to 0.004 to optimize the simulation of d excess over Antarctica (section 3.1.1).

[13] Given the simplicity of the land surface parameterization in LMDZ4, no information is available about the fraction of the evapo,transpiration flux arising from fractionating evaporation (e.g., evaporation of bare soil [*Barnes and Allison*, 1988]). We thus assume no fractionation during

the evapotranspiration over land, as done in most other GCMs [e.g., *Hoffmann et al.*, 1998; *Lee et al.*, 2007]. The coupling with the more detailed land surface scheme ORCHIDEE [*Ducoudré et al.*, 1993; *Rosnay and Polcher*, 1998; *Krinner et al.*, 2005] will be reported in a subsequent paper.

[14] The implementation of water-stable isotopes in the convective scheme has been extensively described by *Bony et al.* [2008]. We pay particular attention to the representation of the reevaporation and diffusive exchanges as the rain falls, which is significantly different compared to other GCMs. While the proportion of the drop that reequilibrates isotopically is prescribed in many GCMs [e.g., *Hoffmann et al.*, 1998], here the relative proportion of evaporative enrichment and diffusive equilibration is calculated depending on relative humidity following *Stewart* [1975]. In addition, the model takes into account the evolution of the compositions of both the rain and the surrounding vapor as the rain drops reevaporate [*Bony et al.*, 2008]. However, when the relative humidity is 100% we simply assume total reequilibration between raindrops and vapor, contrary to *Stewart* [1975] and *Lee and Fung* [2008], who take into account the raindrop size distribution in this particular case.

2.3. Simulations

2.3.1. AMIP Simulations

[15] A first 1979–2007 simulation has been performed following the AMIP protocol [*Gates*, 1992], using prescribed monthly and interannually varying SST and sea ice and a constant CO_2 value of 348 ppm. We allowed a spin-up time of 17 months before January 1979. This simulation is named "free." Another simulation, named "nudged," uses the same protocol but was nudged by the three-dimensional horizontal winds from ERA-40 reanalyses [*Uppala et al.*, 2005] until 2002 and operational analyses thereafter. We did not notice any discontinuity associated with this change in the nudging data set. The simulated wind fields are relaxed toward the reanalyzed winds with a time constant τ = 1 h, so that each component of the horizontal wind field u verifies the following differential equation:

$$\frac{\partial u}{\partial t} = \sum_{i=1}^{n} U_i + \frac{u_{obs} - u}{\tau}$$

where u_{obs} is the reanalysis wind and U_i are the temporal tendencies of each of the n dynamical and physical packages in the model.

[16] The 17 month spin-up time seems to be enough to reach an equilibrium: for example, in the nudged simulation, the globally and annually average $\delta^{18}O$ in precipitation for 1979 is −7.56‰, very close to the average value over 1979–2007 of −7.55‰ compared to the range of interannual variability of 0.06‰ over 1979–2007.

2.3.2. Sensitivity Tests

[17] Sensitivity tests to tunable parameters in the physical or isotopic parameterization have been performed on 3 year simulations with climatological SST, with a spin-up of 17 months. The sensitivities to parameters discussed in this paper are much larger than the interannual variability, justifying shorter simulations that are computationally less expensive than the AMIP 1979–2007 simulations.

[18] Additional 6 year simulations have been performed using the same protocol, but with uniform SST perturbations (as suggested by *Cess and Potter* [1988]): −4 K, −2 K, and +2 K. The sea ice distribution is not modified consistently with the SST in these simulations, but we restrict their analysis to tropical regions in this paper.

2.3.3. Past Climate Simulations

[19] As suggested by the Paleoclimate Model Intercomparison Project (PMIP) project [*Joussaume and Taylor*, 1995; *Braconnot et al.*, 2007] and as in other isotopic modeling studies [e.g., *Jouzel et al.*, 2000], we perform past climate simulations for two periods: the Last Glacial Maximum (LGM, 21 ka) and the Mid-Holocene (MH, 6 ka). For both these periods, a large amount of data is available for model evaluation. These simulations are 5 years long, with a spin-up of 17 months.

[20] A first LGM simulation was performed following a protocol similar to PMIP1 [*Joussaume and Taylor*, 1995], using the Climate: Long-Range Investigation, Mapping, and Prediction (CLIMAP) [*CLIMAP Project Members*, 1981] SST and sea ice, a CO_2 concentration of 180 ppm, orbital parameters following *Berger* [1978]. We set the sea surface $\delta^{18}O$ to 1.2‰ [*Labeyrie et al.*, 1987] and d to 0‰. Contrary to the PMIP1 protocol, we use the *Peltier* [1994] ICE-5G ice sheet reconstruction (as in the work by *Lee et al.* [2008] and PMIP2 [*Braconnot et al.*, 2007]), which differs from the ICE-4G reconstruction (from *Peltier* [1994], used by *Joussaume and Jouzel* [1993] and *Jouzel et al.* [2000]) in the spatial extent and height of Northern Hemisphere ice sheets. Except for the different ice sheet topography, our simulation is similar to that performed by *Joussaume and Jouzel* [1993], *Jouzel et al.* [2000], and *Werner et al.* [2001].

[21] The MH simulations were performed following the PMIP1 protocol, as in work by *Jouzel et al.* [2000]. The only changes compared to present day are the orbital configuration [*Berger*, 1978] and atmospheric gas concentrations (CO_2 concentration of 280 ppm).

[22] The LGM and MH simulations are compared to the free AMIP simulation, considered as a reference for present day (PD).

[23] The warm tropical SSTs and the extensive sea ice of the CLIMAP reconstruction have been questioned [e.g., *MARGO Project Members*, 2009]. Therefore, as in work by *Lee et al.* [2008], we perform an additional simulation using the SST and sea ice simulated by a coupled model (here the IPSL model [*Marti et al.*, 2005] for LGM conditions. We use here the climatological SST from an LGM simulation performed under the PMIP2 protocol (*Braconnot et al.* [2007], with LGM orbital configuration and a CO_2 concentration of 185 ppm), averaged over 50 years. However, significant SST biases in the IPSL model are common to all climate conditions, including LGM and PD. Therefore the direct comparison between SSTs simulated for LGM by the IPSL model ($T_{LGM/IPSL}$) and SSTs observed at PD (T_{PD}) is misleading: SST biases in the IPSL model could be confused with LGM-PD signals. To circumvent this problem, we use the SSTs from an IPSL model pre-industrial simulation (PI) simulation, performed following the PMIP2 protocol (with present-day orbital configuration and a CO_2 concentration of 280 ppm). We force our additional LGM simulation with $T'_{LGM/IPSL} = T_{LGM/IPSL} - T_{PI} + T_{PD}$. This way, the biases in the IPSL model common to both the

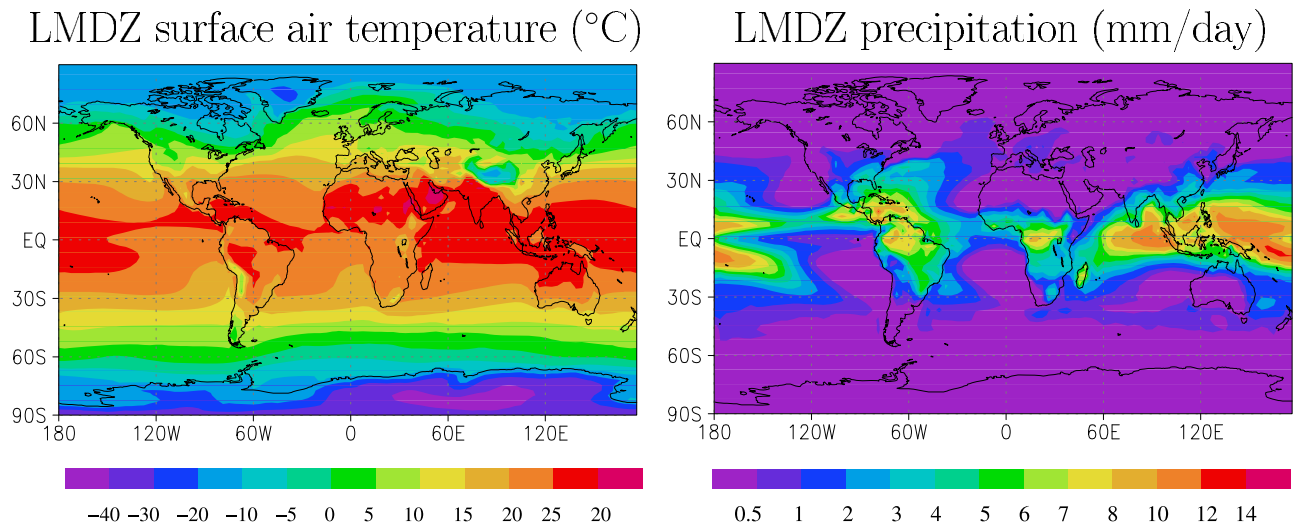

Figure 1. Annual mean (left) temperature and (right) precipitation in the LMDZ-iso nudged simulation.

LGM and PI simulations are canceled out. We can thus compare our LGM isotopic simulations from both CLIMAP and IPSL SSTs in a consistent way.

3. Evaluation and Sensitivity Tests

[24] The present-day climate simulated by LMDZ4 has been extensively evaluated by *Hourdin et al.* [2006]. The mean annual temperature and precipitation maps in the nudged simulation are given in Figure 1 for reference. We focus here on the isotopic simulation. First, we examine the isotopic spatial and seasonal distribution, then its variability at synoptic to interannual time scales in the present-day climate, and finally we evaluate isotopic variations associated with past climates.

[25] We present an evaluation of $\delta^{18}O$, expressed in permil, defined as

$$\delta = \left(\frac{R_{\text{sample}}}{R_{\text{SMOW}}} - 1\right) \cdot 1000,$$

where R_{sample} and R_{SMOW} are the ratio of HDO or $H_2^{18}O$ over $H_2^{16}O$ in the sample and the Standard Mean Ocean Water (SMOW) reference, respectively. At first order, variations in δD follow the same patterns as $\delta^{18}O$ but are 8 times larger. The deviation to this behavior is quantified by the deuterium excess: $d = \delta D - 8 \cdot \delta^{18}O$ [*Dansgaard*, 1964]. This second-order parameter is known to be more difficult to simulate by GCMs [*Lee et al.*, 2007; *Mathieu et al.*, 2002]. We thus present an evaluation of this parameter as well, which is expected to provide stronger constraints on the simulated hydrological and isotopic processes.

3.1. Evaluation of the Spatial and Seasonal Distributions

[26] We use in this section the whole AMIP simulations averaged over the period 1979–2007 to produce average seasonal cycles. We compare the spatial distribution and seasonal cycle with the Global Network of Isotopes in Precipitation (GNIP) data [*Rozanski et al.*, 1993], to which we add data from Antarctica (compiled by *Masson-Delmotte et al.* [2008]) and Greenland (compiled by *Masson-Delmotte et al.* [2005b]). Note that since we compare point data with simulated values averaged over a GCM grid box, the scale mismatch may contribute to the model data difference.

3.1.1. Annual Mean Spatial Distribution of Isotopes in Precipitation

[27] The spatial distribution of annual mean $\delta^{18}O$ in precipitation ($\delta^{18}O_p$) is well simulated in the model, featuring the well-known "effects" [*Rozanski et al.*, 1993]: enhanced depletion with decreasing temperature ("temperature effect"), increasing altitude ("altitude effect") or continentality ("continental effect"), or precipitation intensity ("amount effect") (Figure 2). The $\delta^{18}O_p$ over central Greenland and Antarctica is however overestimated, owing to an overestimated temperature over Antarctica (minimum annual temperature over Antarctica of −42°C in nudged LMDZ-iso and −60°C in the work by *Masson-Delmotte et al.* [2008]). This warm bias is frequent in GCMs [*Masson-Delmotte et al.*, 2006] and is worsened when nudging the model with meteorological reanalyses. The temperature effect in Antarctica is, however, relatively well reproduced, with a spatial slope of 0.73‰/K (r = 0.95) in the data and 0.65‰/K in the model (r = 0.97) over the temperature range simulated by LMDZ-iso (Figure 3).

[28] The deuterium excess in precipitation (d_p) is of the right order of magnitude over most regions except on tropical continents (simulated d_p too high by up to 10‰ over equatorial Africa and northern South America). LMDZ-iso reproduces the d minimum over high-latitude oceans [*Uemura et al.*, 2008] and features a relationship with δD consistent with observations over Antarctica (Figures 3 and 4). LMDZ-iso also captures the d_p maximum over the Middle East, as was also the case in other GCMs [*Hoffmann et al.*, 1998; *Schmidt et al.*, 2007]. LMDZ-iso simulates the spatial distribution reasonably well compared to other GCMs: *Yoshimura et al.* [2008] report spatial correlations between 0.39 and 0.52 between observed and simulated annual d_p values in four isotopic GCMs; LMDZ-iso value is 0.45. However, d_p is slightly underestimated by

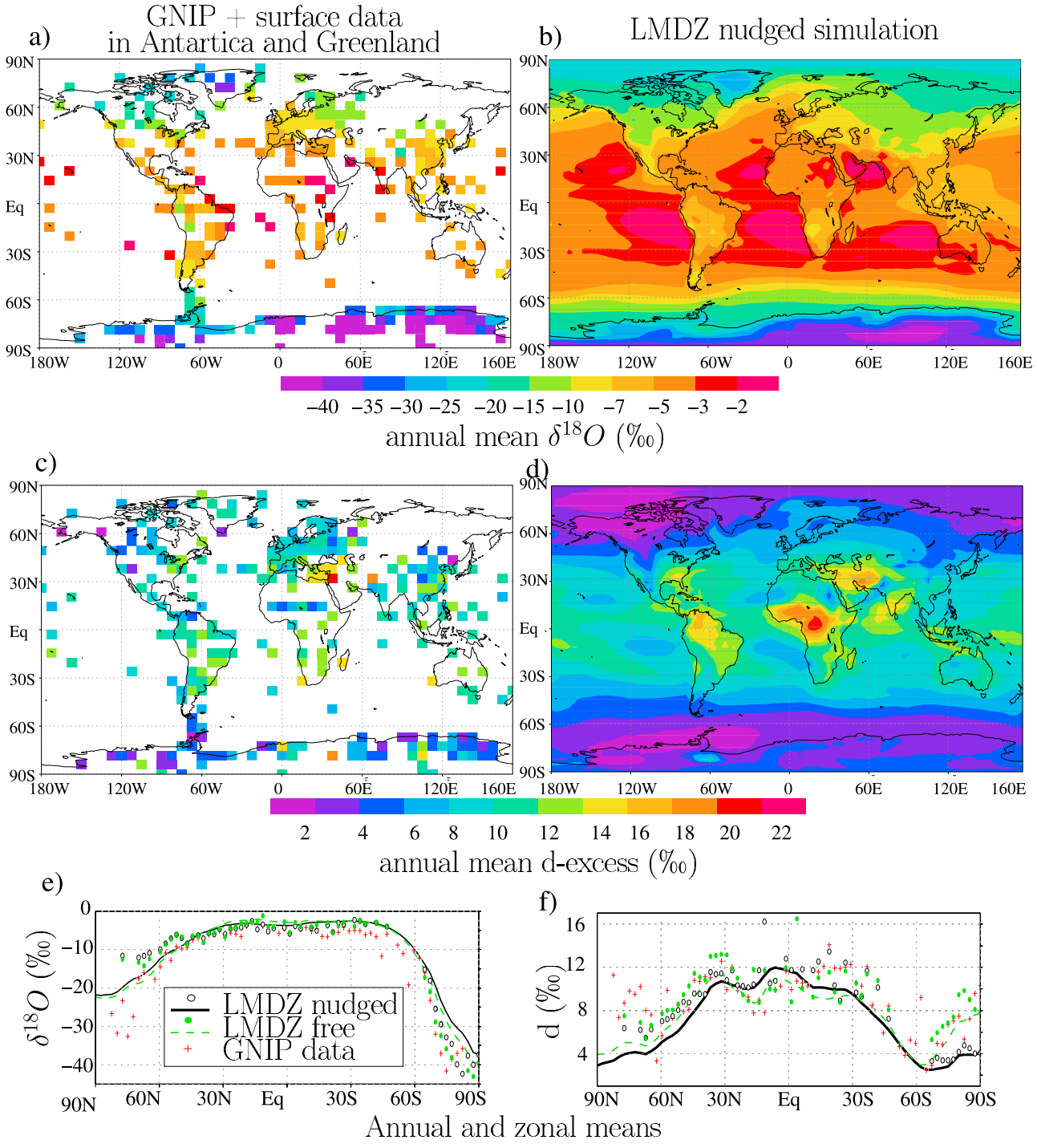

Figure 2. (a, b) Annual mean $\delta^{18}O$ and (c, d) d excess in precipitation, in the data (Figures 2a and 2c) and the LMDZ-iso nudged simulation (Figures 2b and 2d). The data are the GNIP data [*Rozanski et al.*, 1993], the Antarctica data from *Masson-Delmotte et al.* [2008], and Greenland surface data [*Masson-Delmotte et al.*, 2005b]. The data are gridded over a coarse 7.5 × 6.5° grid for visualization purpose. The simulation is the nudged simulation averaged over the 1979–2007 period. Zonal means of the annual averages of (e) δ^{18}O and (f) d excess for the data (red crosses), the nudged simulation (solid black curve), and the free simulation (dashed green curve). The lines are zonal averages for LMDZ-iso simulations, and the points are the values at data stations.

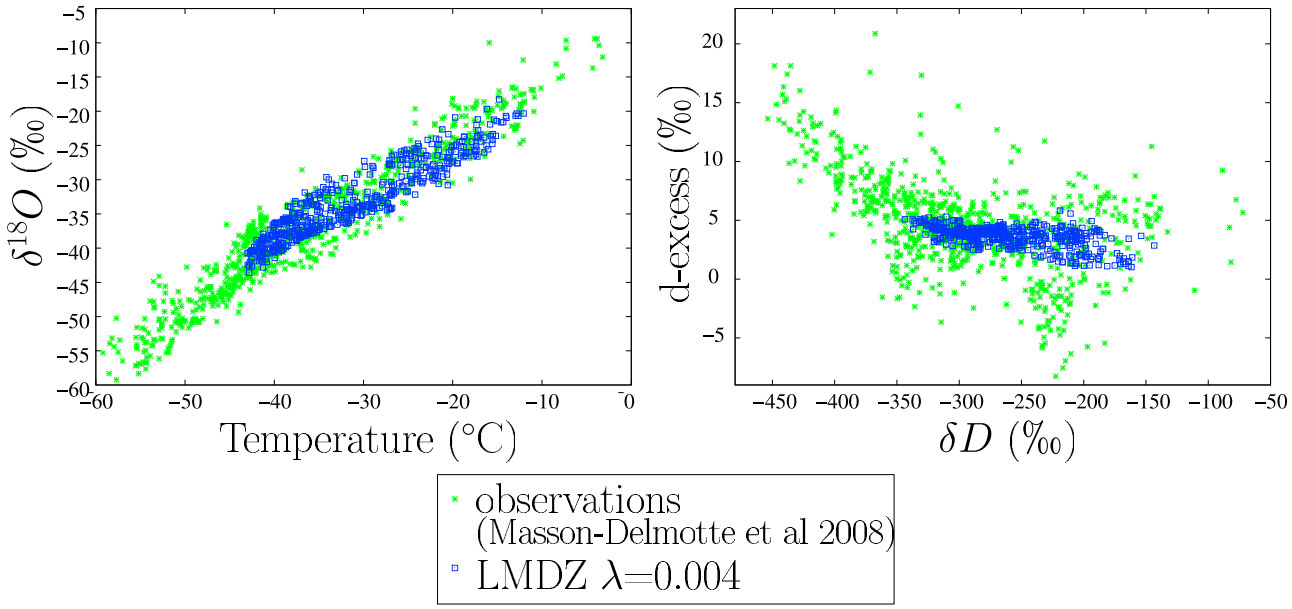

Figure 3. (left) Annual mean δD as a function of annual mean air temperature at first level and (right) annual mean d excess as a function of annual mean δD in precipitation, in the data from *Masson-Delmotte et al.* [2008] (green) and in the LMDZ-iso nudged simulation (blue).

LMDZ-iso at high latitudes, in particular over northwestern America, the Arctic Ocean, and central Antarctica. It is slightly overestimated in convective regions of tropical South America and Africa. Regional patterns in d_p over the tropics differ strongly among the models, in particular over continents. The GISS fully coupled model [*Schmidt et al.*, 2007] and the ECHAM atmospheric GCM [*Hoffmann et al.*, 1998], for example, do not show higher d_p values over South America than over the surrounding oceans, contrary to LMDZ-iso and GNIP. The difference seems unrelated to the representation of fractionating evaporation at the land surface, which is absent in both LMDZ-iso and ECHAM. Instead, it might reveal a different simulated response of d_p to convective activity, which is known to differ between continents and oceans [*Nesbitt and Zipser*, 2003; *Liu and Zipser*, 2005].

[29] The parameter λ, controlling kinetic effects during snow formation, is known to have a strong impact on the d of snowfall in Antarctica [*Jouzel and Merlivat*, 1984; *Schmidt et al.*, 2005]. Typical values for λ are 0.002 [e.g., *Landais et al.*, 2008], 0.003 [e.g., *Hoffmann et al.*, 1998; *Noone and Simmonds*, 2002a] or 0.004 [e.g., *Schmidt et al.*, 2007; *Vimeux et al.*, 2001; *Stenni et al.*, 2001]. In LMDZ-iso, setting λ to 0.002 leads to very strong d_p values over central Antarctica (up to 28‰), whereas setting λ to 0.004 gives results more consistent with the data (Figure 4).

3.1.2. Seasonal Cycles of Isotopes in Precipitation

[30] Figure 5 compares the observed and simulated seasonal cycles of temperature, precipitation, $\delta^{18}O_p$ and d_p over five GNIP stations representative of various climatic conditions (Table 1): Reykjavik (northern Atlantic), Vienna (central Europe), Manaus (Amazon), Apia (western tropical Pacific) and Ankara (Eastern Mediterranean). The seasonal cycles of $\delta^{18}O_p$ are generally well reproduced by LMDZ-iso, especially in the nudged simulation.

[31] On the other hand, the seasonal cycles of d_p are unequally reproduced for the different stations. The performance of LMDZ-iso in simulating the seasonal cycle of d_p is in line with the other GCMs: *Yoshimura et al.* [2008] report a correlation between 0.05 and 0.62 between

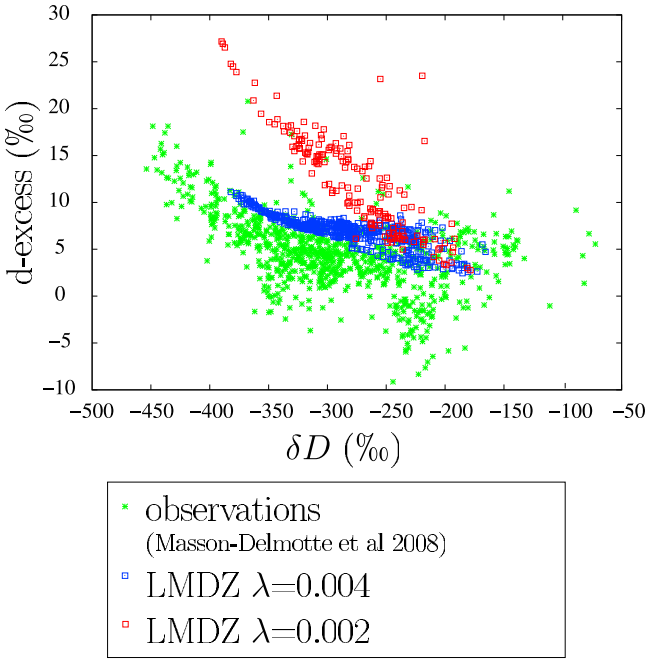

Figure 4. Annual mean d excess as a function of annual mean δD in precipitation in Antarctica, in the data from *Masson-Delmotte et al.* [2008] (green) and in LMDZ-iso free simulations (blue and red). In blue, the supersaturation λ was set to its standard value of 0.004, whereas in red, it was set to 0.002.

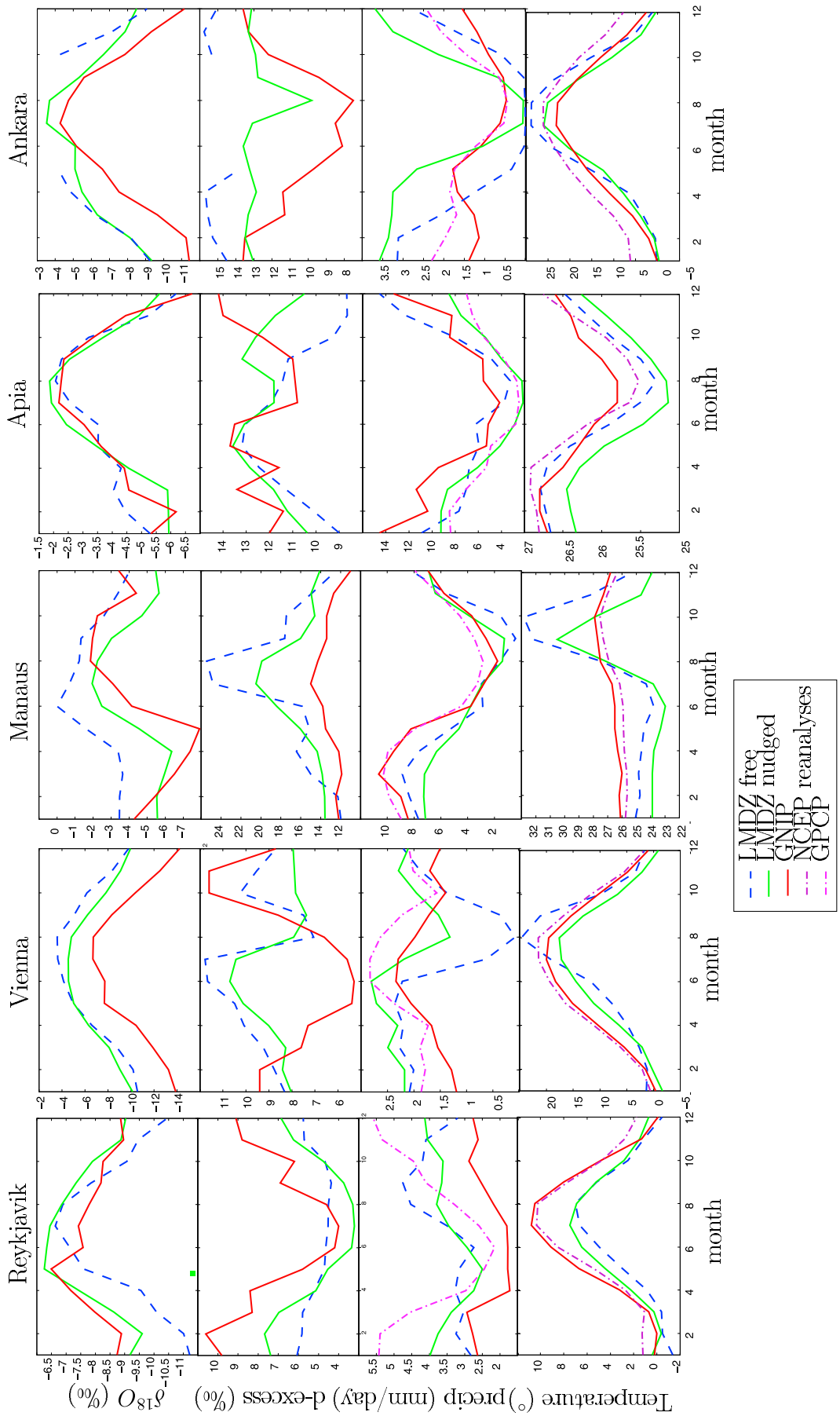

Figure 5. Monthly δ^{18}O and d excess in precipitation, precipitation rate, and temperature over Reykjavik, Vienna, Manaus, Ankara, and Apia for the GNIP data (red) and the LMDZ-iso nudged (green) and free simulations (blue), as well as NCEP [*Kalnay et al.*, 1996] temperatures and GPCP [*Huffman et al.*, 1997] precipitation (pink). Monthly averages are calculated over the 1979–2007 period for LMDZ-iso, NCEP, and GPCP and over the years available for GNIP (Table 1). For LMDZ-iso, we plot the value of the grid box containing the station.

Table 1. Name, Location, and Active Years of the GNIP Stations Chosen to Assess Seasonal Cycles and Interannual Variability of the Isotopic Composition of the Precipitation[a]

Name	Latitude	Longitude	Region	Active Years	Vapor Sampling
Reykjavik	64.13	−21.93	northern Atlantic	1961–2001	-
Vienna	48.25	16.37	central Europe	1961–2001	2001–2003, weekly sampling
Manaus	−3.12	−60.02	central Amazon	1966–1990	1978–1980, monthly sampling
Apia	−13.8	−171.78	western tropical Pacific	1962–1977	-
Ankara	39.95	32.88	eastern Mediterranean	1963–2001	2001–2002, subweekly sampling
Bangkok	13.73	100.50	Southeast Asia	1968–2001	-

[a]"Vapor sampling" gives the frequency and active years of the vapor sampling on some of these stations.

observed and simulated mean June–July–August and December–January–February (JJA-DJF) d_p values in four isotopic GCMs; the LMDZ-iso value is 0.52. At high latitudes, LMDZ-iso simulates everywhere d_p in antiphase with $\delta^{18}O_p$, in agreement with the Reykjavik data (Figure 5) or inland Antarctica [*Fujita and Abe*, 2006] (not shown). But LMDZ-iso is not able to reproduce the phase shift of a few months observed between $\delta^{18}O_p$ and d_p in some stations of coastal Antarctica or Greenland [*Johnsen et al.*, 1989; *Ciais et al.*, 1995; *Delmotte et al.*, 2000]. Over the Mediterranean region, LMDZ-iso simulates an almost flat seasonal cycle of d_p, at odds with the lower d_p observed in summer in Turkey (Ankara, Figure 5) or in Israel [*Angert et al.*, 2008] (not shown). Over the Amazon, LMDZ-iso is able to simulate the maximum of d_p observed during the dry season (e.g., Manaus, Figure 5), though the simulated maximum value is 6‰ too high. During the dry season, simulated d_p values increase with continentality as one goes inland, in agreement with observations [*Salati et al.*, 1979; *Gat and Matsui*, 1991; F. Vimeux et al., manuscript in preparation, 2010]. These features have been interpreted as the effect of fractionating continental recycling (e.g., evaporation from lakes, bare soil [*Salati et al.*, 1979; *Gat and Matsui*, 1991; *Henderson-Sellers et al.*, 2001]). It is thus surprising that LMDZ-iso is able to simulate these features without fractionation during evapotranspiration from land. Processes controlling the seasonal cycle of d_p in South America in LMDZ-iso seem more related to rain-vapor equilibration processes. The reasons for d_p South American cycles in LMDZ-iso, and whether they are the same as in nature, will be investigated in the future.

[32] The amount effect (which refers to the decrease of $\delta^{18}O_p$ with increasing precipitation that is observed in the tropics) is well reproduced by LMDZ-iso (Figure 6): over the nine oceanic tropical stations used by *Bony et al.* [2008], the amount effect is −0.5‰/mm/d in LMDZ-iso compared to −0.7‰/mm/d in the data. The Single Column Model (SCM) of *Bony et al.* [2008], which shares a very similar version of the Emanuel convective parameterization and the same isotopic representation of droplet evaporation, simulates too depleted a precipitation in humid conditions and too strong an amount effect (Figure 6, blue). *Bony et al.* [2008] hypothesized that this bias could be due to the very simple framework of the SCM, in which horizontal isotopic gradients were neglected. Figure 6 confirms this hypothesis: in nature as in LMDZ-iso, the horizontal moisture advections of air masses of different isotopic composition in LMDZ-iso thus act to dampen the amount effect.

3.1.3. Evaluation of the Vapor-Precipitation Equilibrium

[33] A large uncertainty in the representation of water-stable isotopes in GCMs is the representation of isotopic exchanges between vapor and rain droplets as the rain falls and partially reevaporates [*Lee and Fung*, 2008]. The ECHAM GCM, for example, assumes that a constant fraction of the droplet reequilibrates with the vapor, depending on the cloud type [*Hoffmann et al.*, 1998]. Here we calculate explicitly the relative effect of evaporation and equilibration, but we still rely on a tunable parameter ϕ, controlling the relative humidity at the droplet contact, and thus the intensity of kinetic effects: the relative humidity at the droplet contact is parametrized as $\phi + (1 - \phi) \cdot h$, where h is the relative humidity of the vapor reservoir in which droplets reevaporate. Results are very sensitive to this parameter, especially in dry regions where the reevaporation is strong and kinetic effects are crucial: the stronger the kinetic effects, the more the rain gets enriched by evaporation for a given reevaporated fraction [*Bony et al.*, 2008]. This parameter was set to 0.9 by *Bony et al.* [2008]. When setting ϕ to 0 (i.e., reducing the relative humidity at the droplet contact), then the amount effect becomes much stronger and the d_p much lower in dry regions (Figure 7). In LMDZ-iso as in the SCM, the optimal value for ϕ is 0.9.

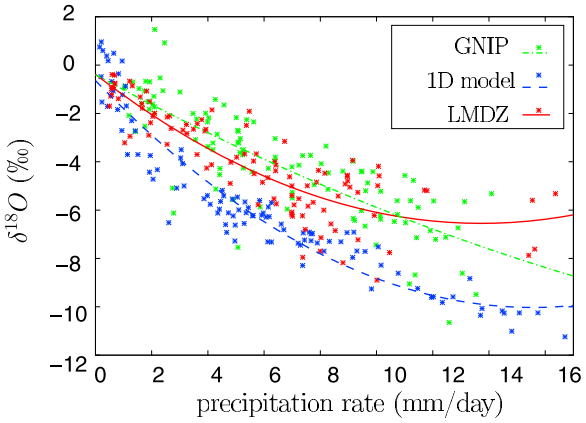

Figure 6. Monthly $\delta^{18}O$ in precipitation as a function of precipitation rate for the nine ocean tropical GNIP stations selected by *Bony et al.* [2008] for the GNIP data (dash-dotted green curve), the LMDZ-iso nudged simulation (solid red curve), and the single-column model of *Bony et al.* [2008] (dashed blue curve). Curves are second-order polynomial fits.

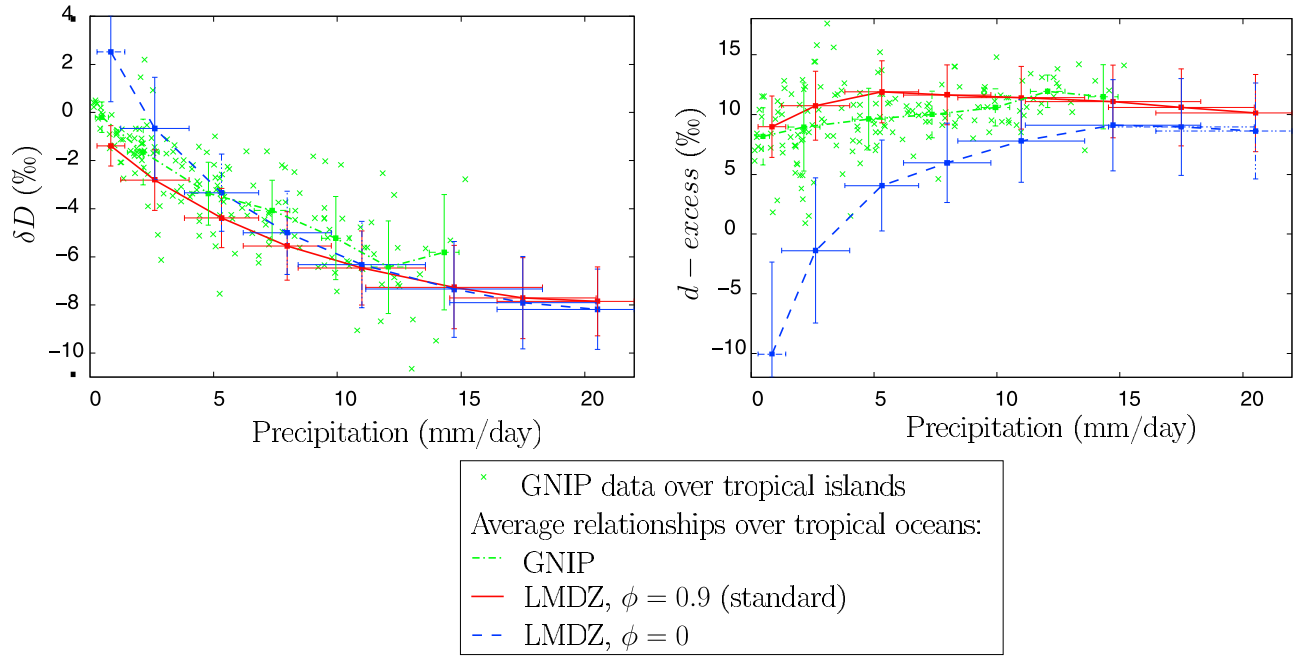

Figure 7. Average relationship between precipitation rate and (left) δ^{18}O and (right) d excess of tropical oceanic precipitation, at the monthly scale, for GNIP data (dash-dotted green curve), and 3 year LMDZ-iso simulations with ϕ set to 0.9 (solid red curve) and to 0 (dashed blue curve). Error bars indicate the standard deviation in each precipitation bin.

[34] As an evaluation of the representation of isotopic processes during evaporation, we compare the degree of equilibration between the vapor and the precipitation at a few stations: Vienna, Manaus, and Ankara, where low-level vapor isotopic compositions are available from the GNIP database at http://nds121.iaea.org/wiser/ (Table 1 and Figure 8). We average both the precipitation and the vapor for all the years available both for the model (1979–2007) and the data (Table 1) to yield monthly averages. Caution is necessary for two sources of uncertainties in the model-data comparison, in addition to possible uncertainties in the data. First, vapor samples were not collected every day and thus may not be representative of monthly averages, given the significant variability observed in the vapor at the daily time scale [e.g., *Angert et al.*, 2008]. However, the relatively smooth seasonal cycles suggest that these data are suitable for a first evaluation of rain-vapor disequilibrium (Figure 8). To estimate this source of uncertainty, we resampled the LMDZ-iso results on the days of observations (Figure 8, dotted green). Second, the precipitation and the vapor samples are not necessarily from the same years. The interannual variability in LMDZ-iso at the three stations is on the order of 1‰ for $\delta^{18}O_v$ and d_v (where $\delta^{18}O_v$ and d_v are the δ^{18}O and d of the vapor), 2‰ for $\delta^{18}O_p$ and up to 3‰ for d_p. We will thus focus on variations in composition exceeding both the standard deviation of measurements within a month for the vapor data (Figure 8) and the typical interannual variability.

[35] In the data over all stations, the rain is more enriched than the low-level vapor ($\delta^{18}O_p - \delta^{18}O_v$ ranges from +7 to +20‰), but over Vienna and Manaus the rain is more depleted (by up to 6‰) than would be expected if the rain was in complete equilibrium with the vapor. This might suggest that the rain, which formed at higher altitude from depleted vapor, reequilibrates only partially. Over Ankara during the dry summer, on the other hand, the rain is more enriched (by about 2‰) than expected from total diffusive equilibration. This suggests some significant evaporative enrichment in dry air. These features are qualitatively well reproduced by LMDZ-iso.

[36] The d_p observed over Vienna and Ankara is lower than in the vapor and lower than would be expected from equilibrium with the vapor (4 up to 19‰ lower). This low d_p could arise from the evaporation of the rain drops as they fall [*Dansgaard*, 1964]. LMDZ-iso strongly underestimates this disequilibrium. It underestimates d in the vapor (d_v), whereas d_p is of the right order of magnitude. This mismatch could arise from (1) a problem in the representation of the kinetic effects during rain evaporation and isotopic exchanges or (2) difficulties in comparing surface vapor samples with an average over a GCM layer (about 20 hPa or 200 m) if some surface processes have an influence restricted to the first few meters above the surface. Over Manaus on the other hand, observed d_p is generally higher than would be expected from equilibrium with the vapor. This could arise from low rain reevaporation in a wet atmosphere. This behavior is qualitatively well captured by LMDZ-iso, but the noisiness of the data limits any deeper analysis.

[37] This calls for more vapor measurements to better constrain and evaluate the representation of isotopic processes during rain fall.

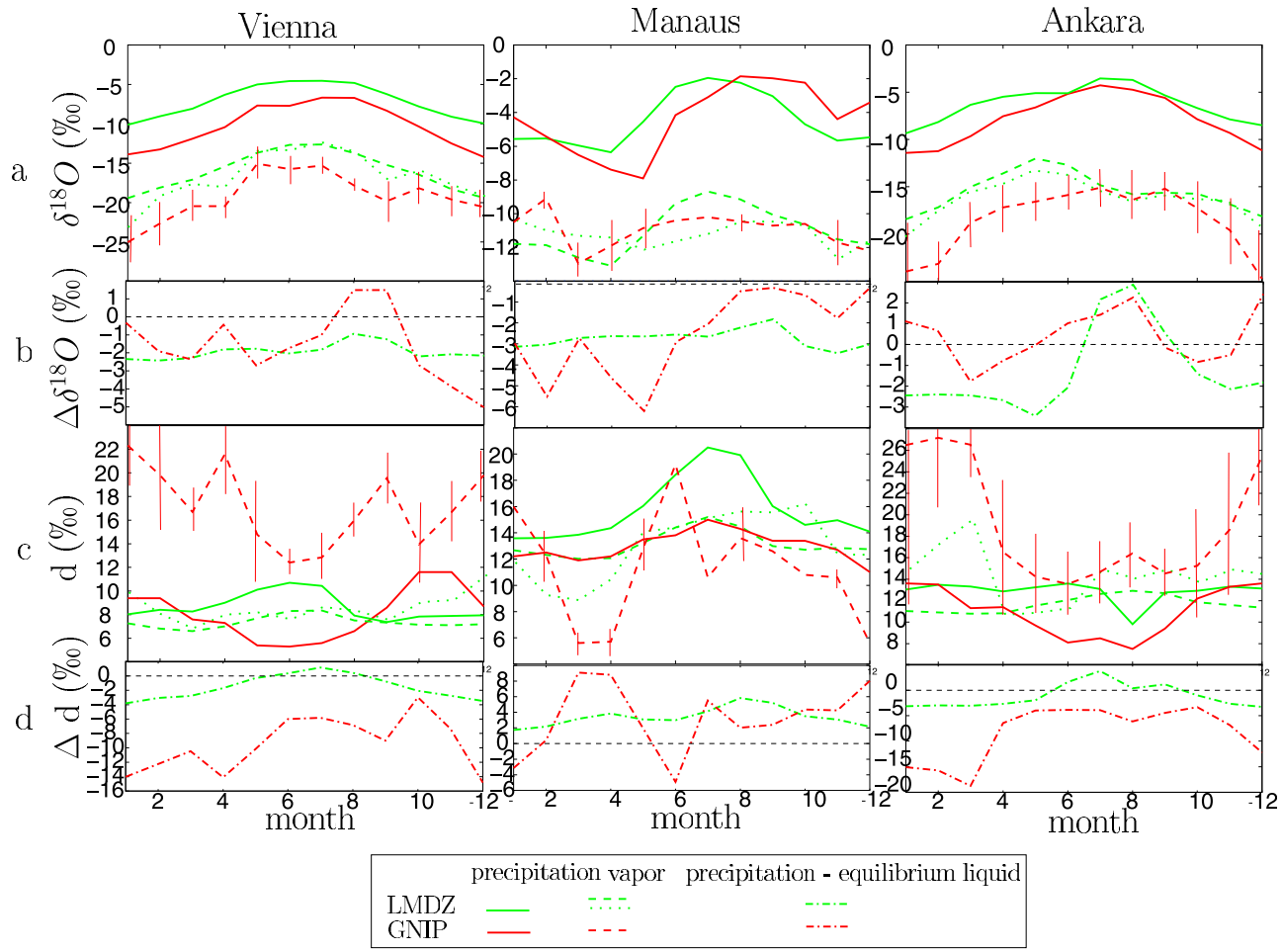

Figure 8. (a) Monthly δ^{18}O in precipitation (solid curves) and vapor at the lowest level (dashed curves) over Vienna, Manaus, and Ankara for the GNIP-vapor data (red curves) and the LMDZ-iso nudged simulation (green curves). For the simulated vapor composition, the dotted green curves show the LMDZ results sampled on the same days as GNIP vapor measurements, whereas the dashed lines show the monthly means. (b) Difference between δ^{18}O in precipitation and the δ^{18}O of a liquid that would be in equilibrium with the vapor, for the GNIP-vapor data (red curve) and the LMDZ-iso nudged simulation (green curve). For LMDZ, the monthly means were used. (c) Same as Figure 8a but for d excess. (d) Same as Figure 8b but for d excess. The error bars for the GNIP vapor data correspond to the standard deviation for the different measurements available for a given month.

3.2. Evaluation of the Isotopic Variability at the Synoptic Scale

[38] In this section, we evaluate the ability of the nudged simulation to simulate the variability at the daily and weekly scale. Unless the model is nudged, the model generates its own weather variability uncorrelated to observations, restricting the evaluation to statistics [*Hoffmann et al.*, 1998; *Noone and Simmonds*, 2002a]. Nudging with reanalyzed winds enables a more rigorous evaluation of the isotopic variability at the synoptic scale [*Yoshimura et al.*, 2008]. Here we present an evaluation using unpublished daily data of both vapor and precipitation collected at the surface at the station of Saclay (near Paris, France, 48.73°N, 2.17°E) from September 1982 to September 1984. Vapor was collected by continuous sampling on a daily basis (except during weekends for which the sampling period covers about 3 days). A cryogenic trap was used, and samples were analyzed for δ^{18}O and δD with an overall accuracy of ±0.15‰ and ±1‰, respectively.

[39] The model reproduces the temperature evolution very well (Figure 9a), especially in winter, when the variability is mainly controlled by large-scale synoptic disturbances. The correlation between observed and modeled daily temperatures is 0.84 in winter and 0.51 in summer. Consistently, the daily variability of $\delta^{18}O_v$ is well captured, especially in winter: the correlation between observed and modeled daily $\delta^{18}O_v$ is 0.65 in winter and 0.46 in summer. However, the temporal slope of $\delta^{18}O_v$ versus temperature at the daily scale in winter is underestimated by the model (0.2‰/K in LMDZ-iso and 0.6‰/K in the data). For example, while LMDZ-iso simulates accurately the strong negative temperature and precipitation anomaly during the first three weeks of February 1983, the corresponding anomaly in $\delta^{18}O_v$ is underestimated by a factor of 2. The mismatch

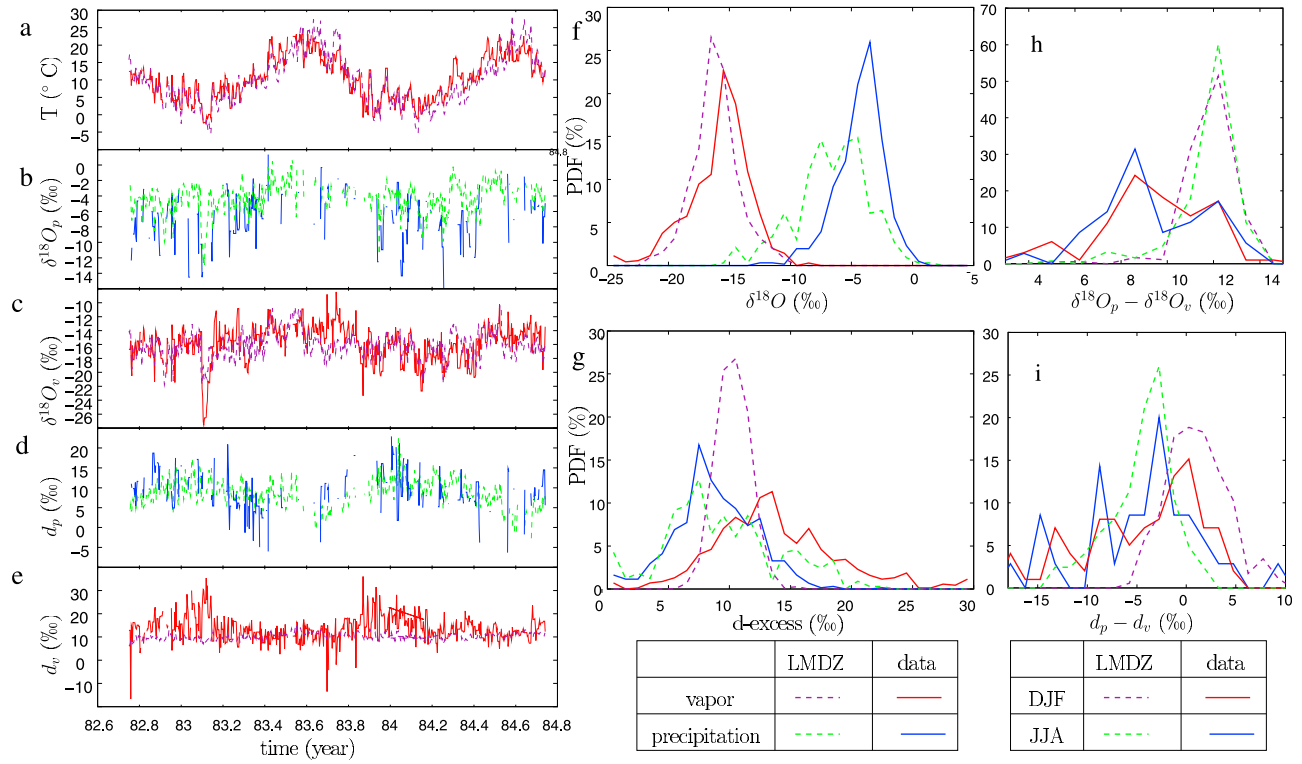

Figure 9. Comparison of the synoptic variability of water isotopes simulated by LMDZ-iso with that observed at the surface in Saclay (near Paris, France, 48.73°N, 2.17°E) from September 1982 to September 1984. Daily evolution of (a) temperature, (b) $\delta^{18}O_p$, (c) $\delta^{18}O_v$, (d) d_p, and (e) d_v. Probability density function of the daily (f) $\delta^{18}O$ and (g) d for all months, in both vapor and precipitation. Probability density function of the daily difference (h) between $\delta^{18}O$ in the precipitation and the vapor and (i) between d in the precipitation and the vapor. Observed temperatures are solid purple curves, measured $\delta^{18}O_v$ and d_v are dashed purple curves, $\delta^{18}O_p$ and d_p are dashed green curves, and LMDZ-iso $\delta^{18}O$ is solid red curve and d is solid blue curve.

could be due to an insufficient distillation of air masses due to a misrepresentation either of the water cycle along the air mass trajectories, or of the trajectories themselves, since LMDZ-iso is not able to simulate the observed 10% decrease in relative humidity during the same period (not shown). This low $\delta^{18}O_v$ event was also underestimated in a nudged simulation by the regional model REMO-iso [*Sturm*, 2005].

[40] The isotopic reequilibration between precipitation and vapor is relatively well reproduced by LMDZ-iso, with the $\delta^{18}O_p$ most frequently 12‰ higher than the vapor in LMDZ-iso and 10‰ in the data.

[41] Although the model satisfactorily simulates the frequency distribution and seasonal variability of d_p, it poorly simulates its synoptic variability (correlation of 0.14 between data and model in winter). The reequilibration between precipitation and vapor for d is well reproduced, with d most frequently 2‰ lower in average in precipitation than in the vapor in LMDZ-iso and about 5‰ lower in the data. This difference between d_p and d_v is strongly sensitive to parameter ϕ controlling kinetic effects during rain re-evaporation: if ϕ is set to 0 (not shown), the simulated d_p is about 8‰ lower than d_v.

[42] The model completely misses the observed variability in d_v, simulating a nearly constant d_v of 10‰ all year round. The correct simulation of d_p is however surprising, suggesting that a good representation of the variability of d_v is not necessary to correctly simulate the variability of d_p. We speculate that some processes near the surface influence d_v in the data, but these processes have no impact on the observed precipitation. The inability of LMDZ-iso to simulate the observed variability in d_v is independent of the vertical resolution: in the standard version of LMDZ-iso (19 levels), the lowest layer is 200 m thick, but there is no improvement in the simulation when using a better vertical resolution (39 levels) with a 35 m thick lowest layer (not shown). This suggests that some processes impacting near-surface d_v are not represented in LMDZ-iso, such as small-scale land surface heterogeneities.

[43] LMDZ-iso, when nudged by reanalyses, can thus satisfactorily simulate the day-to-day variability in temperature that is related to large-scale atmospheric disturbances, and the associated $\delta^{18}O$ variability in vapor and precipitation (at least qualitatively). At the synoptic scale, as is the case at the seasonal scale, the variability in d is more difficult to simulate than that of $\delta^{18}O$. The d_v is even more difficult to simulate than d_p, possibly owing to a mismatch between the scale of in situ measurements and the scale of atmospheric phenomena that can be simulated by a GCM, as was already pointed for the seasonal scale (section 3.1.3).

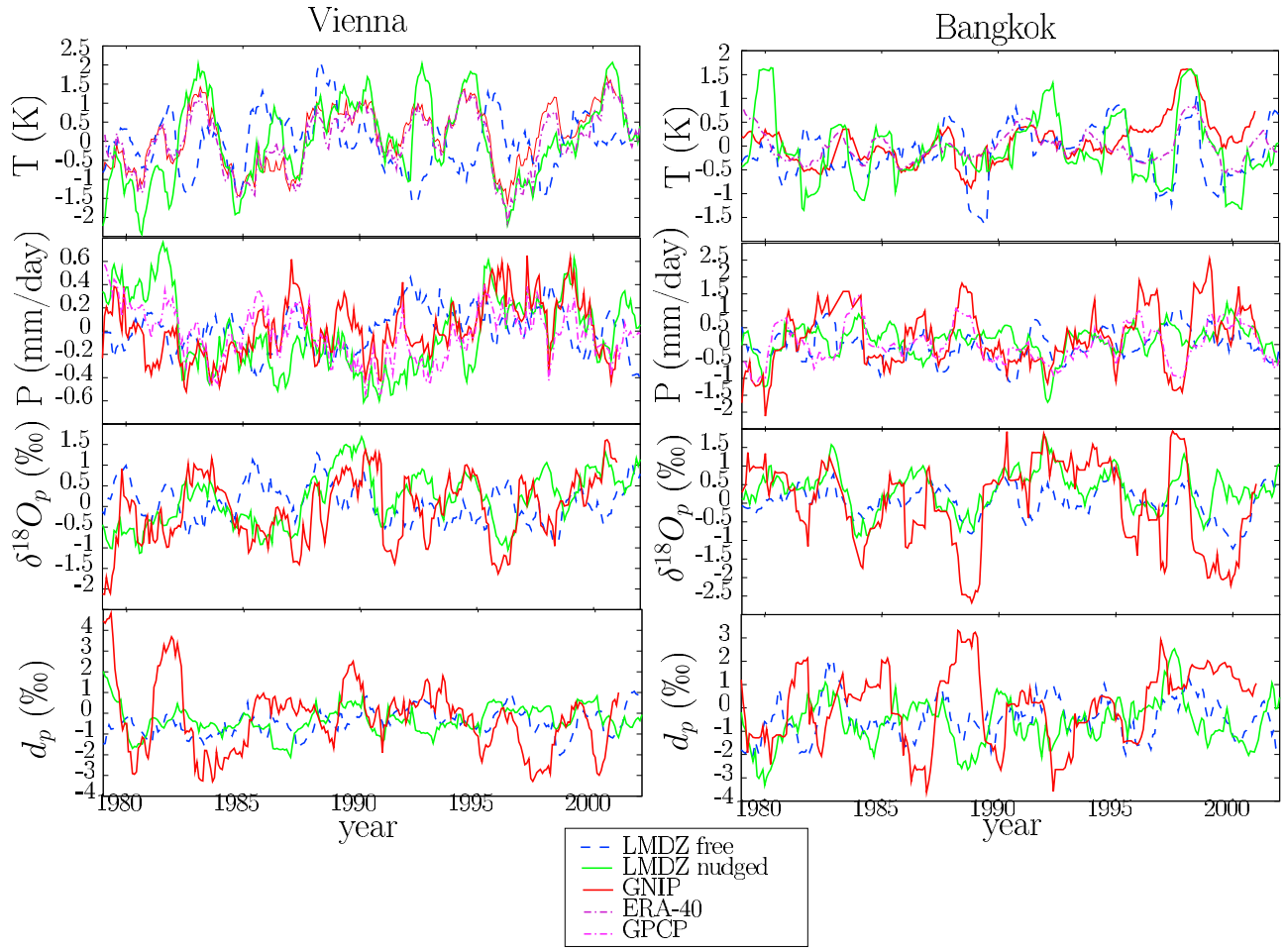

Figure 10. Monthly interannual anomaly of air temperature, precipitation rate, δ^{18}O, and d excess in precipitation over the (left) Vienna and (right) Bangkok GNIP stations, comparing GNIP data and the LMDZ-iso nudged simulation.

Measurements of d_v within the bulk of the boundary layer or at the top of a mat would be more comparable to LMDZ-iso simulations.

3.3. Evaluation of the Isotopic Variability at the Interannual Scale

[44] Water isotopes have been shown to record interannual to decadal variability of the precipitation in the tropics [*Hoffmann*, 2003; *Ramirez et al.*, 2003] and modes of variability in the extratropics such as the North Atlantic Oscillation [*Baldini et al.*, 2008; *Sodemann et al.*, 2008] or the Southern Annular Mode [*Noone and Simmonds*, 2002b]. To evaluate whether LMDZ-iso could be used in the future to study such issues, we evaluate the representation of the isotopic variability at the interannual scale.

[45] The simulation nudged by reanalyzed winds simulates better than the free simulation the interannual variability in temperature, precipitation, and isotopes, as can be shown by time series (Figure 10) over Vienna and Bangkok. These two stations were chosen for their long records and contrasting climate (as in work by *Yoshimura et al.* [2008]) The improvement is particularly strong in midlatitudes. For example, the correlation is 0.80 between model and data monthly anomalies of temperatures (filtered with a 6 month running mean) over Vienna in the nudged simulation compared to 0.05 in the free simulation. Consistently, the variability of $\delta^{18}O_p$ is strongly improved at this station (0.66 compared to 0.26). The simulated variability of precipitation is also improved (0.51 compared to 0.09). On the other hand, in the tropics, the variability in temperature, precipitation, and $\delta^{18}O_p$ is not much improved, consistent with the results of *Yoshimura et al.* [2008]: correlations between model and data $\delta^{18}O_p$ are 0.52 and 0.58 for the nudged and free simulations, respectively. Since tropical SSTs exert a dominant control on the tropical interannual variability, this variability is already well captured by LMDZ-iso just by forcing with observed SST, and the nudging provides little added value. In all simulations, the simulated d_p variability is completely different from the observed variability (correlations of −0.02 and −0.14 over Vienna and Bangkok in the nudged simulations). Also, the interannual variability of d_p is strongly underestimated by LMDZ-iso, as was the case at the synoptic scale.

[46] LMDZ-iso overestimates the correlations of $\delta^{18}O_p$ with both the temperature and the precipitation amount (Figure 11), as pointed out by *Tindall et al.* [2009] for the Hadley model, possibly owing to the different spatial scale of simulations and measurements. LMDZ-iso simulates an

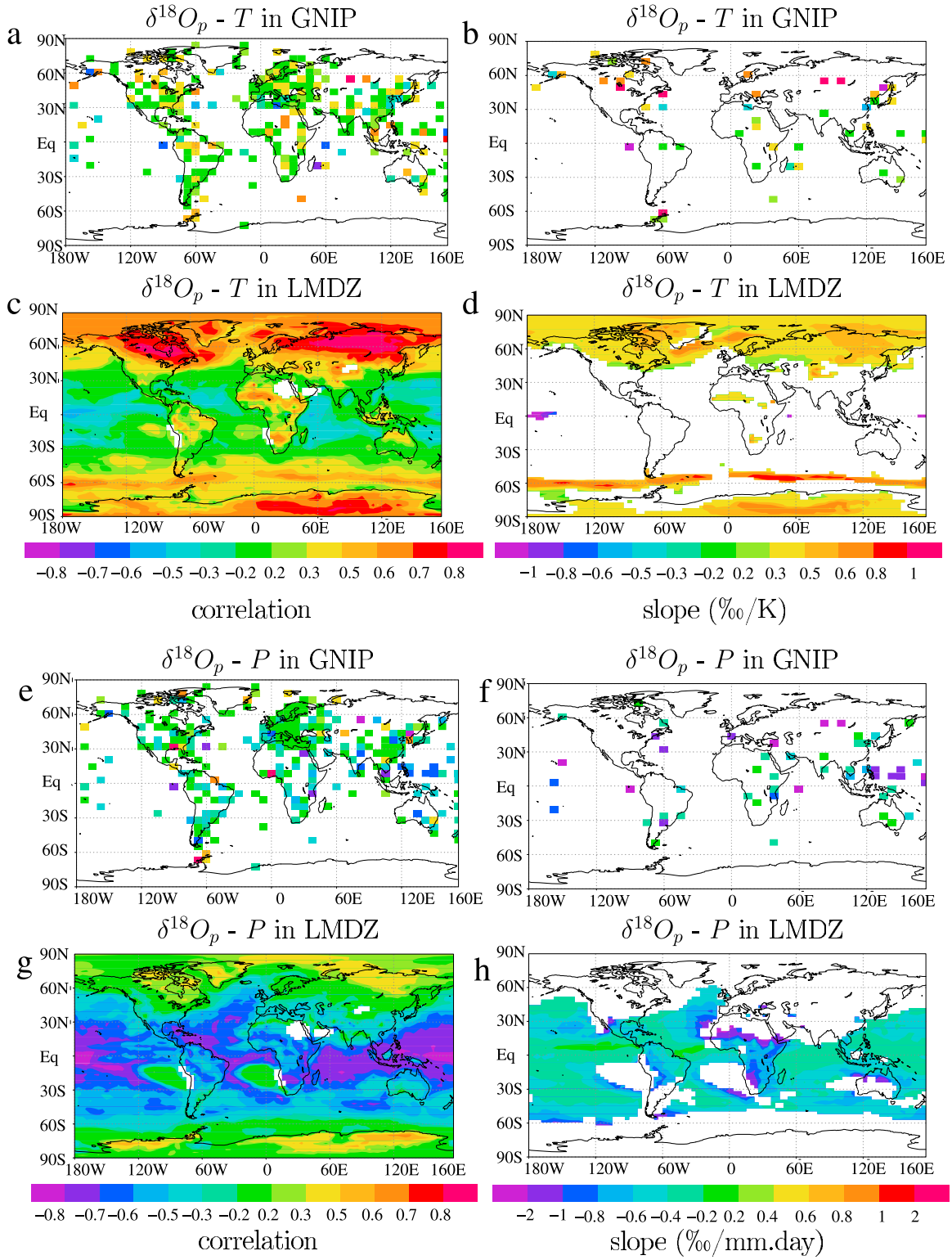

Figure 11. (a, c, e, and g) Correlation coefficients and (b, d, f, and h) slopes of the interannual relationship between monthly anomalies (seasonal cycle subtracted) of $\delta^{18}O$ in precipitation and temperature (Figures 11a–11d) and precipitation rate (Figures 11e–11h). A 6 month running mean was applied to the time series of monthly anomalies before performing the linear regression. The regression is performed for the GNIP data (Figures 11a, 11b, 11e, and 11f) and the nudged 1979–2007 LMDZ-iso simulation (Figures 11c, 11d, 11g, and 11h). White zones correspond to correlations lower than 0.4 in absolute value.

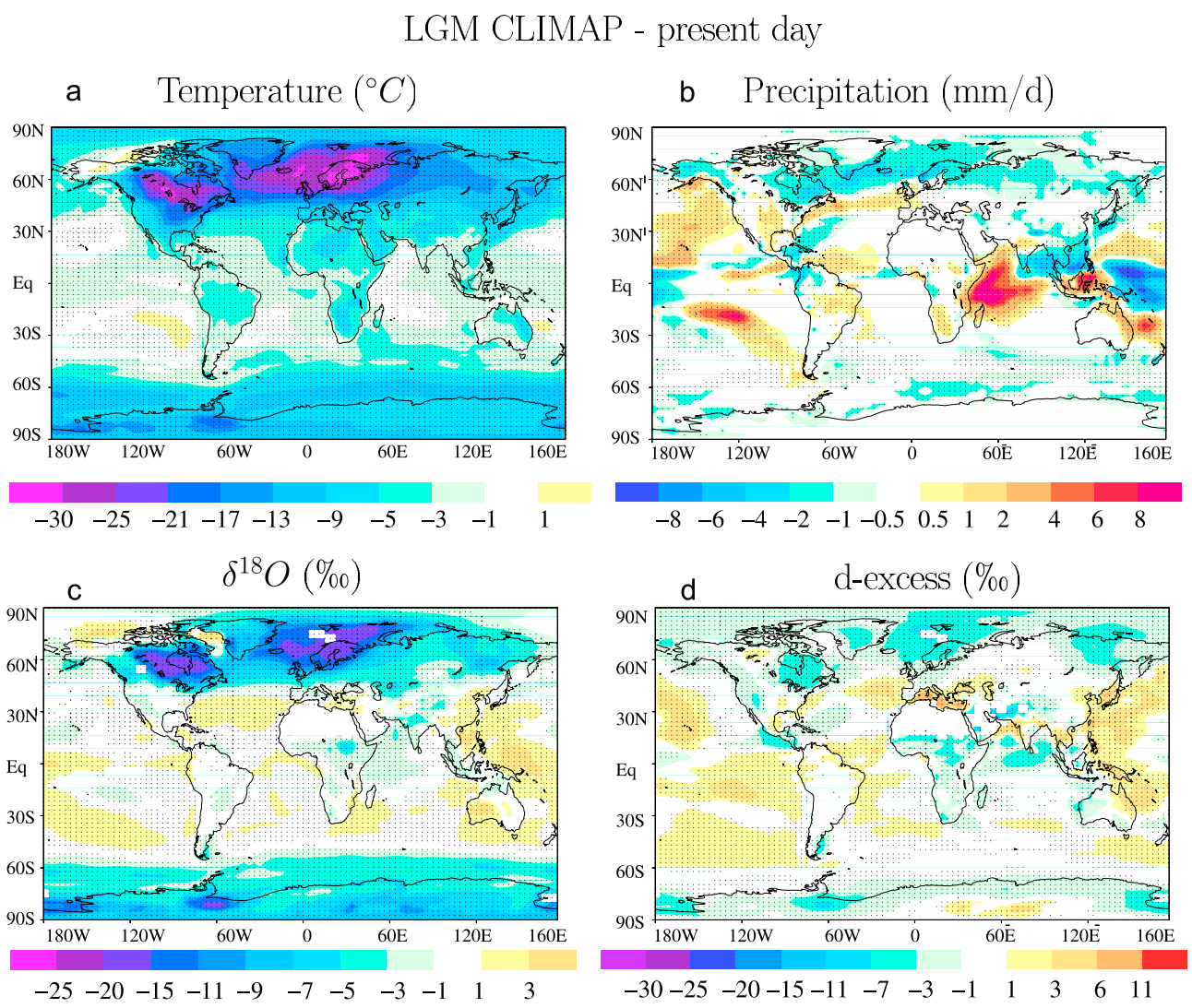

Figure 12. Annual average change between LGM and present day (PD) for (a) temperature, (b) precipitation, (c) $\delta^{18}O$, and (d) d excess. The LGM simulation used the CLIMAP SST [*CLIMAP Project Members*, 1981). Stippling indicates where the LGM-PD difference is stronger than the standard deviation of the interannual variability.

interannual slope of $\delta^{18}O$ versus temperature ranging from 0.3 to 0.8 ‰/K in high latitudes, on the same order of magnitude as those derived from the GNIP data (Figure 11). In the tropics, the simulated amount effect is about −0.5‰/(mm/d), also comparable with GNIP data [*Rozanski et al.*, 1993].

[47] Therefore, LMDZ-iso, when forced by observed SST and nudged by reanalyzed winds, simulates relatively well the interannual variability in $\delta^{18}O_p$, though it has more difficulties in simulating d_p.

3.4. Evaluation of Isotopic Variations at Paleoclimatic Scales

[48] We have seen that LMDZ-iso reproduces reasonably well the present-day climate and its variability from the synoptic, regional scale to the interannual, large scale. In this section, we evaluate the capacity of LMDZ-iso to simulate the isotopic changes associated with two past climates (described in section 2.3.3): the Last Glacial Maximum (LGM) and the Mid-Holocene (MH).

3.4.1. Last Glacial Maximum

[49] Comparing the model results to the data for the LGM is not straightforward. In the case of South American speleothems, for example, the minimum $\delta^{18}O$ values are about −4.5‰ at about 18,000 years before present (18 ka) [*Cruz et al.*, 2006], but values around 21 ka are about −3‰, same as in present day [*Cruz et al.*, 2005b]. Here we consider that the LGM value corresponds to the minimum $\delta^{18}O$ values between 17 and 21 ka, or take the LGM values given by the author. Dating uncertainty could explain the different LGM dates. However, if the minimum $\delta^{18}O$ actually does not occur at the same time at all places (as suggested by some studies [*Smith et al.*, 2005; *Sylvestre*, 2009]), the combination of the LGM data is impossible to simulate with a time slice simulation [*Farrera et al.*, 1999; *Pinot et al.*, 1999], adding an additional source of discrepancy between the model and data.

[50] Figures 12 and 13 show the changes between LGM and PD simulated by LMDZ-iso when forced at LGM by

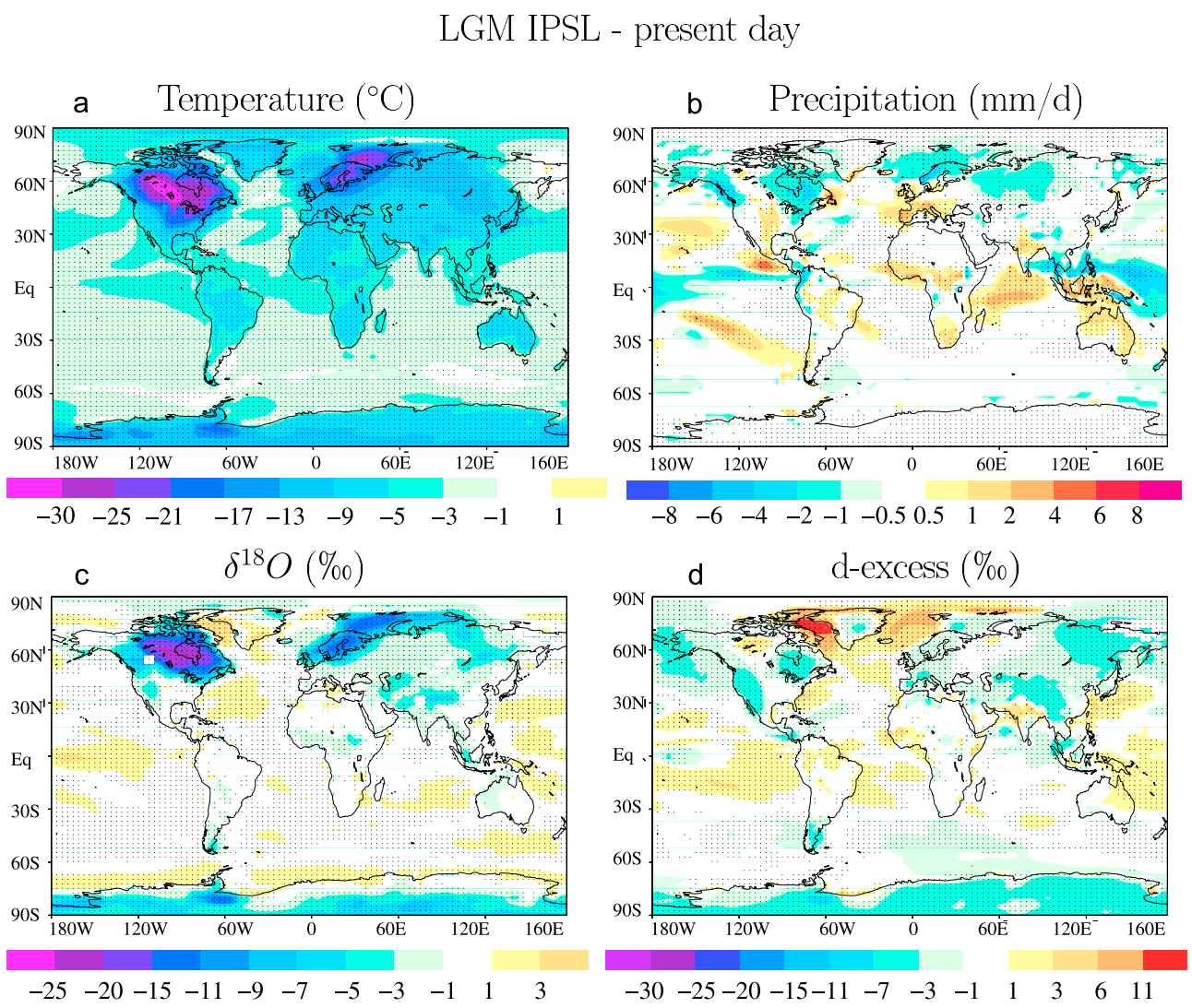

Figure 13. Same as for Figure 12 but for the LGM simulation using the SSTs from an LGM simulation with the coupled IPSL model. The setup of this simulation is detailed in section 2.3.3.

CLIMAP or IPSL SSTs, respectively. Forced by CLIMAP SSTs, LMDZ-iso simulates well the depletion in $\delta^{18}O_p$ over mid and high latitudes during the LGM, except in north-eastern America and over part of the Arctic where a slight enrichment is simulated. Forced by IPSL SSTs, which are up to 10 K warmer than CLIMAP SSTs over high-latitude oceans, LMDZ-iso is able to simulate the depletion observed in ice cores in Antarctica but not in Greenland.

[51] The relevance of spatial slopes for reconstructing paleotemperatures at high latitudes has extensively been discussed [*Jouzel et al.*, 2003; *Lee et al.*, 2008]. In Greenland, the temporal temperature-$\delta^{18}O_p$ slope between LGM and PD (0.3‰/K [*White et al.*, 1997]) has been suggested to be half the spatial slope (0.67‰/K), possibly due to colder source temperatures [*Boyle*, 1997] at LGM or to changes in the seasonality of precipitation [*Krinner and Werner*, 2003; *Werner et al.*, 2000]. This leads to an underestimation by a factor of 2 of temperature changes based on $\delta^{18}O_p$. In Antarctica, on the other hand, studies suggest the temporal and spatial slope are similar with a margin of ±20% [*Jouzel et al.*, 2003; *Krinner and Werner*, 2003], leading to reconstructions of past temperature changes with an error lower than 2°C. This is supported by simulation with the GISS and ECHAM GCMs forced by CLIMAP SSTs: they simulate temporal slopes between LGM and PD in eastern Antarctica on the order of 0.7‰/K and 0.6‰/K, respectively [*Jouzel et al.*, 2003] compared to a spatial slope on the order of 0.75‰/K. On the other hand, the CAM model, when forced by SSTs simulated by a coupled model, simulates temporal slopes half smaller than the spatial slopes in the same region [*Lee et al.*, 2008]. We compare here these results with those from LMDZ-iso forced by the CLIMAP and IPSL LGM SSTs. In Greenland, LMDZ-iso simulates a temporal slope between LGM and PD of about 0.4‰/K over Greenland, half the spatial slope of 0.8‰/K, consistent with earlier studies and all other GCMs [*Jouzel et al.*, 2000]. In Antarctica, LMDZ-iso forced by the CLIMAP SSTs simulates temporal slopes in Vostok of 0.8‰/K, virtually equal to the spatial slope in this region. The simulated temporal slopes are within 20% of the spatial slope over most locations in

Table 2. Data Used for Comparison With the LGM Simulation[a]

Station and Data Type	Latitude	Longitude	Reference	$\Delta\delta^{18}O$ Obs	Δd Obs	$\Delta\delta^{18}O$ LMDZ-iso	Δd LMDZ-iso
GRIP ice core (Greenland)	72.60	−38.5	*GRIP Members* [1993] cited by *Lee et al.* [2008] *Masson-Delmotte et al.* [2005a]	−7	−3	−9.8, +1.9	−3.4, −4
Camp Century ice core (Greenland)	77.17	−61.1	*Johnsen et al.* [1972] cited by *Jouzel et al.* [1994]	−12.9		−4.7, +7.4	−2.3, +8.5
Renland ice core (Greenland)	72	−25	*Johnsen et al.* [1992] cited by *Jouzel et al.* [1994]	−5		−11.9, −2.0	−1.3, −0.4
NGRIP ice core (Greenland)	75.10	−42.32	*NGRIP Members* [2004] cited by *Lee et al.* [2008]	−8		−8.1, +1.5	−3.5, −2.9
England	53	−2	*Bath* [1983] cited by *Joussaume and Jouzel* [1993]	−1.2		−8.1, −3.5	−1.0, −1.2
Vostok ice core (Antarctica)	−78.45	106.85	*Lorius et al.* [1985] cited by *Werner et al.* [2001]	−3 to −5	−2	−6.8, −2.6	−0.2, −4.7
Byrd ice core (Antarctica)	−80.2	−119.5	*Johnsen et al.* [1972] cited by *Lee et al.* [2008]	−8		−6.3, −4.4	−1.4, −2.3
Dome C ice core (Antarctica)	−74.7	124.2	*Lorius et al.* [1979] cited by *Jouzel et al.* [1994] *Stenni et al.* [2001]	−5.4	−4	−6.2, −0.3	−1.3, −5.0
Dome B ice core (Antarctica)	−77.8	94.9	*Vaikmae et al.* [1993] cited by *Jouzel et al.* [1994]	−5		−7.8, −3.3	+0.4, −4.6
Taylor Dome (Antarctica)	−77.8	71.6	*Grootes et al.* [2001] cited by *Lee et al.* [2008]	−3		−6.7, −2.0	+1.6, −4.4
Stampriet aquifer (Namibia)	−25	18	*Stute and Talma* [1998] cited by *Gasse* [2000]	+1.5		−1.5, −0.3	−1.1, −0.5
Huascaran ice core (South America)	−9.11	−77.61	*Thompson et al.* [1995]	−6.3	−4	+1.2, +0.5	+1.2, 0.0
Sajama ice core (South America)	−18.10	−68.97	*Thompson et al.* [1998]	−5.4		−1.1, −1.3	−0.5, −1.0
Illimani ice core (South America)	−16.62	−67.77	*Ramirez et al.* [2003]	−6	−4	−0.4, −0.3	+0.2, +0.2
Botuvera cave (South America)	−27.2	−49.02	*Cruz et al.* [2005b]	−1.5		−1.2, −0.6	+1.0, +1.1
Santana cave (South America)	−24.52	−48.72	*Cruz et al.* [2006]	−1.5		−0.5, 0.1	+0.9, +0.8
Rio Grande do Norte speleothems records (South America)	−5.60	−37.73	*Cruz et al.* [2009]	−0.5		+0.9, −0.3	+0.6, +0.9
Salar de Uyuni (South America)	−20	−68	*Fritz et al.* [2003]	−4		−1.1, −1.3	−0.3, −0.1
Guliya ice core (Tibet)	35.28	81.48	*Thompson et al.* [1997] cited by *Thompson et al.* [2000]	−5.4		−2.2, −5.1	−2.2, −4.9
Dunde ice core (Tibet)	38	96	*Thompson et al.* [1989]	−2		−2.1, −2.3	−0.5, −1.5
Sanbao and Hulu caves (China)	31.67	110.43	*Wang et al.* [2008]	+1.5		−1.6, +0.5	−0.3, −0.8

[a]Name (column 1) and location (columns 2 and 3) of the data stations, reference for the data (column 4), and LGM-PD difference in $\delta^{18}O$ and d excess measured in records (columns 5 and 6) and simulated by LMDZ (columns 7 and 8). We consider as LGM what the author considers as LGM or otherwise take the period of minimum $\delta^{18}O$ in the record between 17 ka and 21 ka. We take an approximate average value over 2 kyr. We take as present day the value averaged over the last 2 kyr. The $\delta^{18}O$ differences in carbonates expressed as PDB were converted in SMOW using $\Delta\delta_{SMOW} \simeq 1.03 \cdot \Delta\delta_{PDB}$ [*Coplen*, 1988]. For LMDZ-iso (columns 7 and 8) the first and second entries in each column are corresponding values for the CLIMAP SST–PD SST and for the IPSL LGM SST–PI, respectively (see section 2.3.3 for simulation setup).

eastern Antarctica, consistently with the GISS and ECHAM simulations reported by *Jouzel et al.* [2003]. On the other hand, when forced by IPSL LGM SSTs, the temporal slopes are most frequently around 0.5‰/K, i.e., 40% lower than the spatial slope. This is in closer agreement with *Lee et al.* [2008], who also used simulated SSTs. This suggests that the controls of $\delta^{18}O_p$ over Antarctica, and thus the accuracy of reconstructions based on present-day spatial slopes, strongly depend on the pattern of SST change. If the change in SST features a strong equator-pole gradient as in CLIMAP, then the spatial slope can be applied to past temperature reconstructions within 20% accuracy. On the other hand, if the SST change has a lower equator to pole gradient, as simulated by the IPSL or CAM coupled models [*Lee et al.*, 2008], then using the spatial slope for temperature reconstruction leads to an underestimation of past temperature changes (by about 40% in the LMDZ-iso simulation forced by IPSL SSTs). At this stage we are more confident in reconstructed than in simulated paleoclimatic SSTs, as large SST pole-equator gradients are confirmed by the recently published MARGO data [*MARGO Project Members*, 2009]. Our results thus rather supports the current use of PD spatial slope to interpret isotopic profiles recovered in central Antarctica.

[52] In the tropics, LMDZ-iso simulates little isotopic change and fails to simulate the depletions ranging from −1.5‰ to −6.3‰ inferred from tropical ice cores and South American speleothems (Table 2). Even when using SSTs from the IPSL coupled model, which are about −2.9 K colder than PD in the tropics, the decrease in $\delta^{18}O_p$ is small (less than 2‰). Temperature does not seem to have any significant effect on tropical $\delta^{18}O_p$ in LMDZ-iso, at any time scale. The failure to simulate lower $\delta^{18}O_p$ in South America is common to other GCMs [*Werner et al.*, 2001; *Jouzel et al.*, 2000]. However, it is not clear whether the depletions measured in available records (Table 2) are representative at the scale of the entire tropics.

[53] Another typical failure of isotopic GCMs for the LGM is their inability to simulate the lower d_p measured in ice cores at high latitudes during LGM [*Werner et al.*,

2001], or more generally to simulate $\delta^{18}O$ and d variations of the same sign on climatic time scales [*Noone*, 2008]. However, LMDZ-iso does simulate a lower d_p over most of Greenland (e.g., Summit: −3.5‰ compared to −3‰ in observations, Table 2), and over most of Antarctica except in central East Antarctica. In the simulation using coupled SSTs, the Antarctic d_p during the LGM is lower than present day by −4‰, in even better agreement with the data. The reason for this behavior of d_p will be the subject of future investigations.

[54] To conclude about the LGM simulations, LMDZ-iso simulates realistic LGM depletions at high latitudes but, like other GCMs, misses the more depleted values measured for LGM at low latitudes. Contrary to other isotopic GCMs [*Werner et al.*, 2001], it simulates a lower d_p in most high-latitude regions, in agreement with the data. However, the CLIMAP LGM simulation still fails to show the lowest glacial d_p over East Antarctica, and the coupled SST LGM simulation generates lower d_p values at the cost of unrealistic high glacial $\delta^{18}O$ values over Greenland.

3.4.2. Mid-Holocene

[55] In agreement with simulations from the GISS and ECHAM models [*Jouzel et al.*, 2000], and in agreement with measurements (Table 3), the isotopic changes between MH and PD are very small in most regions. Exceptions are found, however, over the Sahel, in the Middle East, in central Asia, and in the western United States, where a depletion on the order of 5‰ is simulated (Figure 14).

[56] The monsoon regions are relatively well represented in the LMDZ-iso model, though the precipitation amounts are slightly underestimated in summer [*Hourdin et al.*, 2006]. At orbital time scales, variations in precipitation are antiphased between the hemispheres [*Wang et al.*, 2006; *Kutzbach et al.*, 2008], but this antiphase is not captured by LMDZ. Therefore, LMDZ-iso is not able to reproduce the $\delta^{18}O_p$ changes in monsoon regions that are out of phase between hemispheres [*Cruz et al.*, 2009], but erroneously produces more negative $\delta^{18}O_p$ throughout the entire tropical belt (Figure 14). LMDZ-iso is not able either to reproduce the antiphase observed in $\delta^{18}O_p$ between east and west South America [*Cruz et al.*, 2009].

[57] Still, during the Mid-Holocene, the Indian and African monsoons are enhanced in LMDZ-iso (up to +3 mm/d in annual average), in agreement with other PMIP models [*Joussaume et al.*, 1999]. As a result, the precipitation downstream of these regions of enhanced precipitation is more depleted (up to −8‰ in the Northern Sahel and Tibet), consistent with the amount effect. The corresponding $P - \delta^{18}O_p$ slopes are much higher than at the interannual or seasonal scales. For example, when averaging the western African monsoon precipitation over the 20°W–30°E; 10°N–20°N region [*Joussaume and Taylor*, 1995] and for the July to September months (JJAS), the MH-PD $\delta^{18}O_p$ change ($\Delta\delta^{18}O_p$) is −2.0‰ for a +1.1 mm/d precipitation change (ΔP), leading to a climatic slope ($\Delta\delta^{18}O_p/\Delta P$) for JJAS of −1.7‰/mm/d (much higher than the seasonal or interannual slope of about −0.5‰/mm/d, Figure 11). This climatic slope is even higher when considering annual averages (−5‰/mm/d). This shows that the amount effect may depend on the time scale of variability considered [*Schmidt et al.*, 2007] and that reconstructions of past precipitation based on present-day calibration at the seasonal or interannual scale are to be taken with caution as discussed further in section 4.2.

4. Climatic Information Recorded by Water Isotopes in the Tropics

[58] The precipitation amount dominates the isotopic composition of the tropical precipitation at intraseasonal [*Yoshimura et al.*, 2003; *Sturm et al.*, 2007; *Risi et al.*, 2008b], seasonal [*Dansgaard*, 1964; *Rozanski et al.*, 1993], and interannual scales [*Rozanski et al.*, 1993; *Vuille and Werner*, 2005]. At longer time scales, the interpretation of isotopic records from tropical ice cores has been the subject of debate. *Thompson et al.* [2000] have shown that tropical records from ice cores in South America and Tibet share common $\delta^{18}O$ patterns during the last 25 kyr, with most depleted values during the LGM (by 4 to 6‰) and an increase during the deglaciation. The temporal evolution is also qualitatively similar to higher-latitude records in Greenland and Antarctica [*Thompson et al.*, 2000]. This could suggest a large-scale control of the isotopic signal, which was first interpreted as temperature variations [*Thompson et al.*, 2000]. However, given that the main process controlling low-latitude $\delta^{18}O$ variations at present day is the precipitation amount, these variations have subsequently been interpreted as wetter conditions upstream of ice cores [*Vimeux et al.*, 2009].

[59] Given the ability of LMDZ-iso to reproduce the main features of the observed water isotopic distributions, we now use it to investigate issues related to the interpretation of isotopic records as proxies for past changes in temperature and precipitation. First, we quantify the relative impact of changes in precipitation and large-scale temperature changes on $\delta^{18}O_p$ (section 4.1). We then evaluate the robustness of reconstructions of past precipitation based on water-stable isotopes (section 4.2).

4.1. How Much Do Global Temperature Changes Impact Tropical $\delta^{18}O_p$?

[60] A global temperature change is likely to imprint $\delta^{18}O_p$ over the whole planet. However, if the change in surface temperature is not spatially uniform, the large-scale circulation will also change, which will lead to substantial changes in precipitation. Regional changes in $\delta^{18}O_p$ are thus expected to result both from background temperature and regional circulation changes.

[61] To identify a possible effect of mean temperature on $\delta^{18}O_p$, we perform simulations with uniform changes of SST (−4 K, −2 K, and +2 K). Uniform changes in SST result in uniform shifts in the $\delta^{18}O_p$ probability distribution in the tropics (Figure 15a), by about 0.1 ‰/K. The probability distributions of $\delta^{18}O$ in the vapor and in the evaporation are equally shifted (not shown), suggesting that this small sensitivity to mean SST is mainly due to a change in fractionation during evaporation at the sea surface (a sensitivity of 0.08‰/K is predicted by the *Merlivat and Jouzel* [1979] simple closure assumption). The sensitivity to SST is the same for all uniform SST change experiments (Figure 15b) and consistent with the SCM results of *Bony et al.* [2008]. The LGM simulations are also associated with a decrease in mean $\delta^{18}O_p$. Figure 15c plots $\delta^{18}O_p$ as a function of the

Table 3. Data Used for Comparison With the MH Simulation[a]

Name	Latitude	Longitude	Reference	$\Delta\delta^{18}$O Obs	Δd Obs	$\Delta\delta^{18}$O LMDZ-iso	Δd LMDZ-iso
GRIP Ice Core (Greenland)	72.6	−38.5	*GRIP Members* [1993] cited by *Masson-Delmotte et al.* [2005b]	+0.5	−0.2	−1.3	−0.7
North GRIP ice core (Greenland)	75.10	−42.32	*Masson-Delmotte et al.* [2005b]	+0.7	−0.5	−1.3	−0.7
Vostok ice core (Antarctica)	−78.45	106.85	*Lorius et al.* [1985] cited by *Thompson et al.* [2000]	−0.2		+0.4	−0.6
Byrd ice core (Antarctica)	−80.2	−119.5	*Johnsen et al.* [1972] cited by *Thompson et al.* [2000]	+1		−0.4	−0.5
Huascaran ice core (South America)	−9.11	−77.61	*Thompson et al.* [1995]	0		−0.5	0.8
Sajama ice core (South America)	−18.10	−68.97	*Thompson et al.* [1998]	0		−0.4	−0.2
Illimani ice core (South America)	−16.62	−67.77	*Ramirez et al.* [2003]	+0.2		−1.0	0.0
Botuvera cave (South America)	−27.2	−49.02	*Cruz et al.* [2005b]	+0.5		−1.4	+0.5
Santana cave (South America)	−24.52	−48.72	*Cruz et al.* [2005b]	+1		−1.2	+0.1
Rio Grande do Norte speleothems records (South America)	−5.60	−37.73	*Cruz et al.* [2009]	−3.5		−1.5	+1.6
Tigre Perdido (South America)	−5.9	−77.3	*van Breukelen et al.* [2008]	+0.5		+0.1	+1.2
Guliaa ice core (Tibet)	35.28	81.48	*Thompson et al.* [2000]	−2.5		−0.7	−0.4
Sanbao and Hulu caves (China)	31.67	110.43	*Wang et al.* [2008]	−1.8		−0.4	+0.3

[a]Name (column 1) and location (columns 2 and 3) of the data stations, reference for the data (column 4), and MH–present-day difference in δ^{18}O and d excess measured (columns 5 and 6) and simulated by LMDZ-iso (columns 7 and 8). We take as MH the value at 6 ± 1 ka and for present day the values averaged over the last 2 kyr. The δ^{18}O differences in carbonates expressed as PDB were converted in SMOW using $\Delta\delta_{SMOW} \simeq 1.03 \cdot \Delta\delta_{PDB}$ [*Coplen*, 1988].

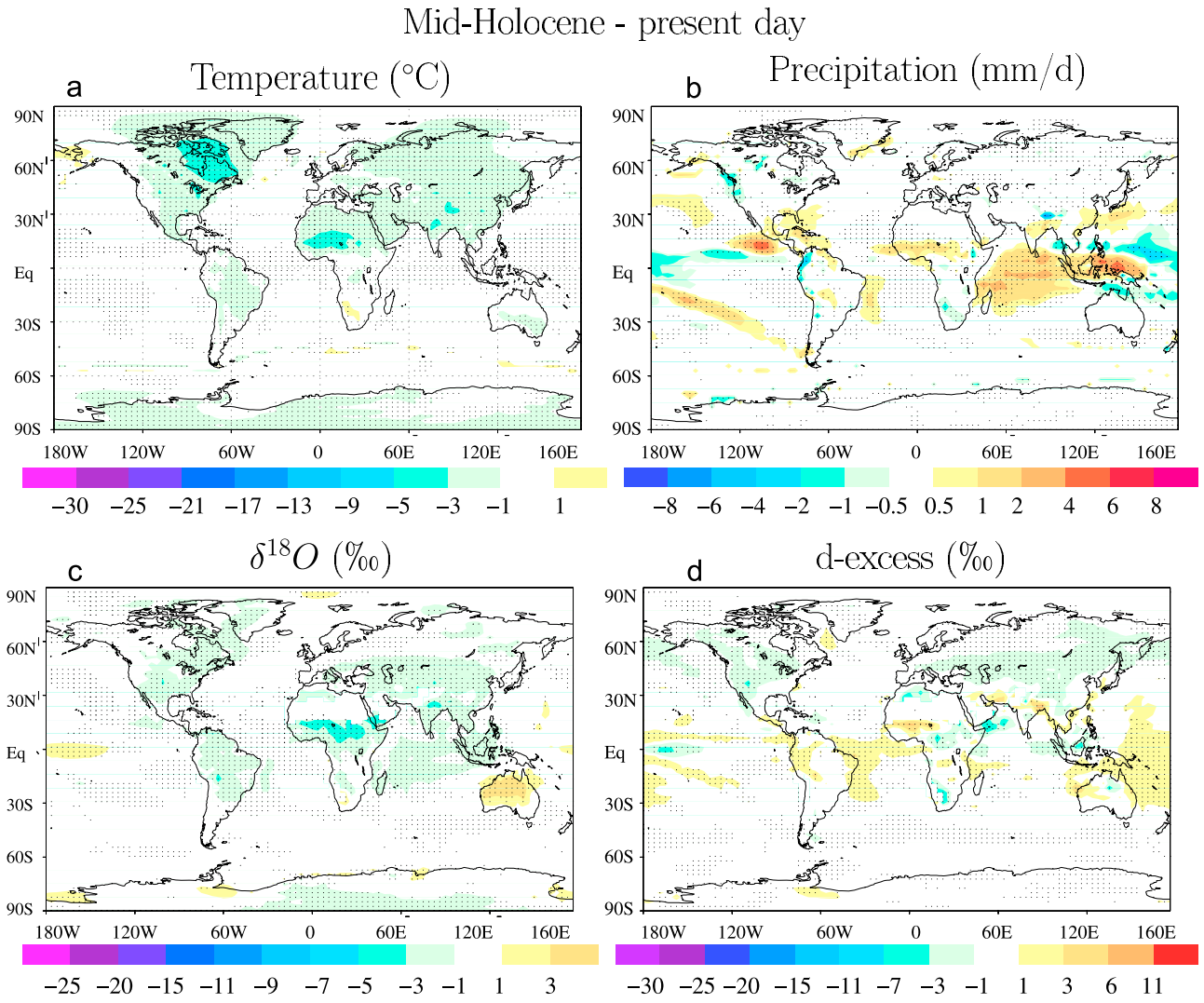

Figure 14. Same as for Figure 12 but for Mid-Holocene minus present day.

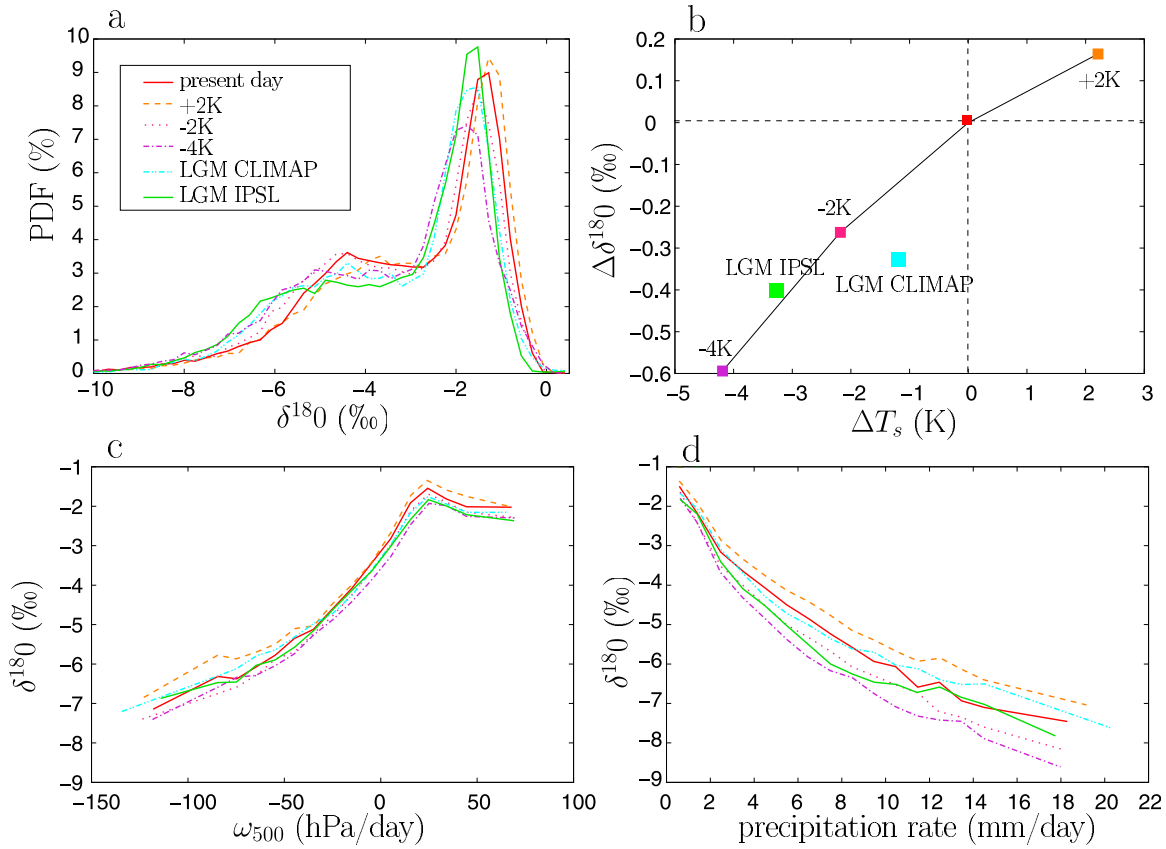

Figure 15. (a) Frequency distribution of the δ^{18}O of precipitation over the tropics (−30°S–30°N) for the different simulations: present day (red), idealized simulation of uniform SST changes, and the two LGM simulations. For each simulation, monthly $\delta^{18}O_p$ values (averaged over the different years of simulation) for all the tropical grid boxes were used. (b) Annually and tropically average change in $\delta^{18}O_p$ (compared to present day) as a function of the annually and tropically averaged change in sea surface temperature. (c) Mean relationship of $\delta^{18}O_p$ over tropical oceans as a function of the large-scale vertical velocity at 500 hPa ω_{500}. For each simulation and in each bin of ω_{500}, we calculate the average $\delta^{18}O_p$ using monthly ω_{500} and $\delta^{18}O_p$ values in all tropical grid boxes. (d) Same as Figure 15c but as a function of the precipitation rate P.

large-scale vertical velocity at 500 hPa, considered as a proxy for dynamical regimes (e.g., large-scale ascent or subsidence [*Bony et al.*, 2004]): the sensitivity to SST is nearly uniform for all dynamical regimes. Therefore, in our GCM, the sensitivity of 0.1‰/K is robust for all types of climate changes and dynamical regimes.

[62] This sensitivity of $\delta^{18}O_p$ to mean SST is smaller than the sensitivity to local temperature measured at high latitudes: temperature-$\delta^{18}O_p$ slopes at high latitudes are about 0.4‰/K at the seasonal scale [*van Ommen and Morgan*, 1997; *Ekaykin and Lipenkov*, 2008] and range from 0.3 to 1‰/K at the interannual scales (Figure 11). Therefore, the sensitivity of $\delta^{18}O_p$ to mean SST in the tropics simulated by LMDZ cannot explain by itself the strong depletion in $\delta^{18}O_p$ measured in the tropics for the LGM. Then, how to interpret the inability of GCMs to reproduce the depletion measured locally in most tropical records? If this is a large-scale mismatch due to an underestimate of the sensitivity of $\delta^{18}O_p$ to mean SST in the tropics, it might reveal a misrepresentation by GCMs of some hydrological or isotopic processes in the tropics. Alternatively, since the largest LGM-PD depletions in the tropics are measured in high-altitude ice cores, the mismatch might be just regional and due to the coarse spatial resolution of GCMs over mountainous regions. However, the coarse resolution may not explain the inability of LMDZ to simulate the 2‰ more depleted precipitation at LGM measured in Brazilian speleothems that are close to the sea level [*Cruz et al.*, 2005a, 2006]. A better spatial coverage of δ^{18}O data at LGM would aid understanding of whether this mismatch is a large-scale or regional feature.

[63] While changes in mean tropical SST have little impact on $\delta^{18}O_p$, the precipitation amount is a dominant control on $\delta^{18}O_p$ in the tropics at the seasonal and spatial scale (Figure 15d). Following the framework of *Bony et al.* [2004], precipitation variations can be decomposed into two components: (1) a dynamical component, due to changes in the large-scale atmospheric circulation associated with changes in the SST distribution, and (2) a thermodynamical component, related to the change in the mean tropical precipitation with mean tropical SST (about 2%/K [*Held and Soden*, 2006]). In LMDZ-iso, a uniform increase in SST leads to both a thermodynamic increase in precipitation and a slight increase in $\delta^{18}O_p$ (Figure 15a), leading to an apparent $P - \delta^{18}O_p$ relationship opposite to the amount

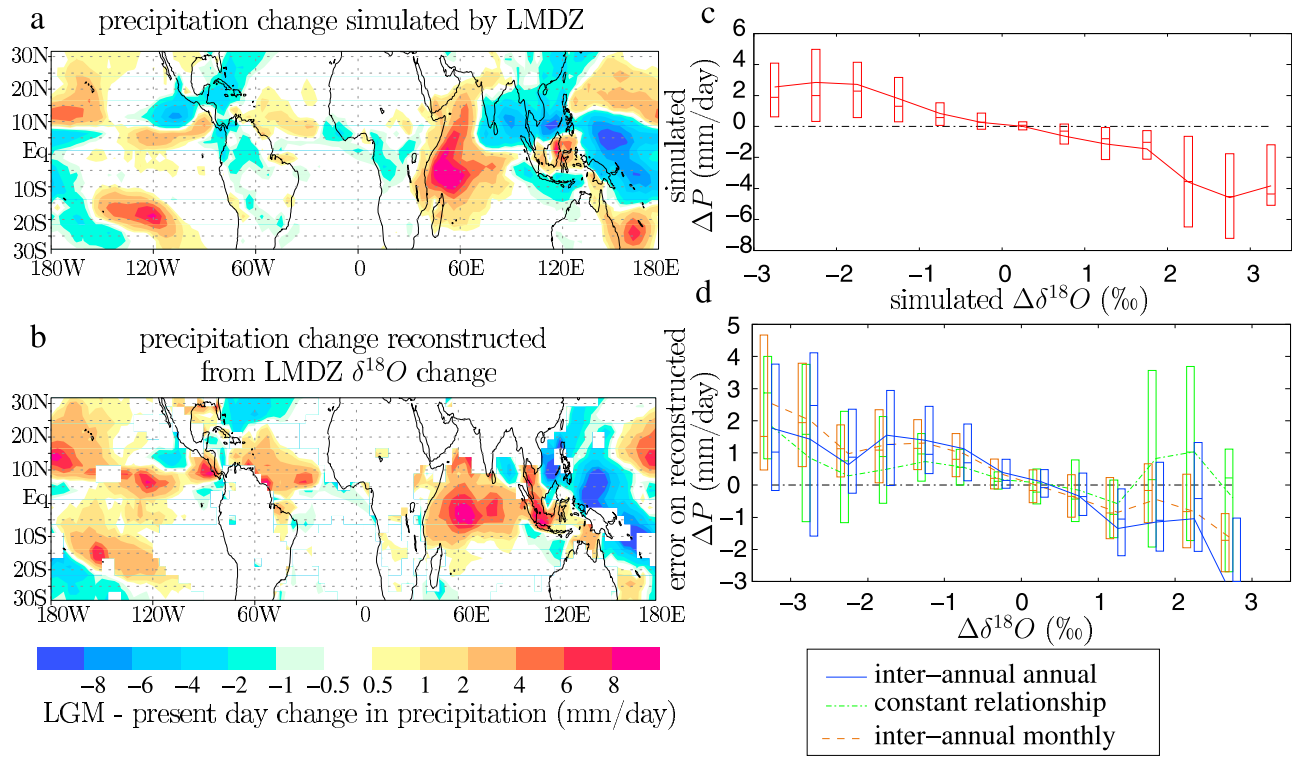

Figure 16. (a) LGM–present-day change in P simulated by LMDZ-iso. (b) LGM–present-day change in P reconstructed from the interannual $\delta^{18}O_p - P$ slope simulated by LMDZ-iso. Areas where the correlation coefficient is higher than −0.25 are white. (c) Annually averaged precipitation change between LGM and PD as a function of the annually averaged change in $\delta^{18}O_p$, simulated by LMDZ-iso, over all tropical locations. The curve shows the average while the bars show the median and quartiles. (d) Error in the reconstructed precipitation change (reconstructed minus simulated by LMDZ-iso) as a function of change in $\delta^{18}O_p$ for different methods: local slope between annual mean precipitation and annual mean $\delta^{18}O$ (dashed blue curve); constant relationship of −0.7‰/(mm/d) (dash-dotted green curve); and local slope between monthly anomalies of $\delta^{18}O_p$ and precipitation, applied on monthly values (dashed brown curve).

effect. The $\delta^{18}O_p$ thus responds only to the dynamical component of the precipitation change, in agreement with a previous SCM study [*Bony et al.*, 2008]. Therefore, the tropical $\delta^{18}O_p$ records mainly regional changes in precipitation related to changes in the large-scale circulation rather than changes in mean temperature or precipitation at the scale of the entire tropics.

4.2. How Much Can We Consider Water Isotopes in Tropical Precipitation as a Good Proxy for Local Precipitation Rate?

[64] In LMDZ-iso, the tropical $\delta^{18}O_p$ records mainly dynamical changes in precipitation. General circulation models simulate precipitation responses to climate change that are very model-dependent, in particular in monsoon regions [e.g., *Held et al.*, 2005]. As the tropical $\delta^{18}O_p$ is closely related to the precipitation amount, the ability of GCMs to reproduce past $\delta^{18}O_p$ changes might help to assess, indirectly, the ability of GCMs to simulate the precipitation response to a global climate change. A prerequisite for this approach, however, is that past local precipitation changes can, indeed, be accurately inferred from water-stable isotopic records. Here, we examine this issue through a "perfect model" experiment, using the CLIMAP LGM and PD simulations: we reconstruct the LGM-PD change in precipitation ($\Delta P_{\text{reconst}}$, Figure 16b) from the LGM-PD $\delta^{18}O_p$ change simulated by LMDZ-iso ($\Delta\delta^{18}O_{sim}$, Figure 12c), and compare this reconstruction with the precipitation change actually simulated by LMDZ-iso (ΔP_{sim}, Figure 16a).

[65] To do so, we first calculate at each grid point the slope of the linear regression (s) of the annual mean $\delta^{18}O_p$ versus annual mean P simulated at the interannual scale by LMDZ-iso. We use annual mean values since the temporal resolution of paleoclimatic records is rarely higher than the year. Then, we reconstruct the precipitation change as $\Delta P_{\text{reconst}} = \frac{1}{s} \cdot \Delta\delta^{18}O_{sim}$, when the coefficient of the linear regression is lower than −0.25, an arbitrary negative cutoff, which ensures that P is indeed a significant control on $\delta^{18}O_p$. Performances of the reconstructions increase as the cutoff decreases, but the relative performances of the different reconstruction methods are insensitive to the choice of the cutoff.

[66] The reconstructed precipitation pattern compares well with the pattern actually simulated by the model (Figures 16a and 16b): the spatial correlation between $\Delta P_{\text{reconst}}$ and ΔP_{sim} is 0.61 (Table 4). The larger the precipitation changes, the better the reconstruction, such as over the Indian Ocean. Where $|\delta^{18}O_p|$ changes are larger than 2‰, 92% of

Table 4. Performance of the Reconstruction of Past Changes in Precipitation Using the Present-Day Interannual Slope of $\delta^{18}O_p$ Versus P in the Perfect Model Experiments[a]

Past Climate	Reconstruction Method	Cutoff	Spatial Correlation	Probability Right Sign $\lvert\Delta\delta^{18}O_p\rvert > 2‰$	Probability Error < 50% $\lvert\Delta\delta^{18}O_p\rvert > 2‰$	Probability Right Sign All Locations	Probability Error < 50% All Locations
LGM CLIMAP	annual	−0.25	0.61	92	29	75	25
LGM CLIMAP	constant	−0.25	0.60	89	34	74	24
LGM CLIMAP	monthly	−0.25	0.74	89	31	71	19
LGM CLIMAP	annual	−0.7	0.68	96	39	81	38
LGM IPSL	annual	−0.25	0.22	72	20	62	14
MH	annual	−0.25	0.62	85	16	72	26
MH	monthly	−0.25	0.59	87	31	73	31

[a]Perfect model experiments are described in section 4.2. We reconstruct changes in precipitation (ΔP) between past climate (column 1) and present day, using different methods (column 2): slope of annual mean $\delta^{18}O_p$ versus annual mean P (annual), constant slope of −0.7‰/(mm/d) (constant), and slope of monthly anomalies of $\delta^{18}O_p$ versus P applied on monthly $\Delta\delta^{18}O_p$ values (monthly). Column 4 gives the spatial correlation between the simulated and reconstructed ΔP. Columns 5 and 7 give the probability that the reconstructed ΔP is of the right sign for locations where $\lvert\Delta\delta^{18}O_p\rvert > 2‰$ and for all locations, respectively. Columns 6 and 8 give the probability that the reconstructed ΔP is within 50% of the simulated ΔP for locations where $\lvert\Delta\delta^{18}O_p\rvert > 2‰$ and for all locations, respectively. All correlations and probabilities are calculated only on locations where the interannual correlation is lower than an arbitrary cutoff (column 3).

the location have $\Delta P_{reconst}$ of the right sign, and 29% of the locations have a reconstructed ΔP relative error (calculated as $(\Delta P_{reconst} - \Delta P_{sim})/\Delta P_{sim}$) smaller than 50% (Table 4). These probabilities decrease to 76% and 25%, respectively, when considering all locations (Table 4). ΔP reconstructions are thus more robust when $\delta^{18}O_p$ variations are larger and thus when the signal to noise ratio is higher. Consistently, reconstructing changes in precipitation is less successful for the Mid-Holocene, for the LGM with IPSL SST, and for uniform SST change experiments, because these simulations show small dynamical changes of precipitation and small $\delta^{18}O_p$ variations. The probability that the relative error in reconstructed ΔP be smaller than 50% at locations where $\lvert\delta^{18}O_p\rvert$ changes are larger than 2‰ is only 20% for the LGM with IPSL SSTs and 17% for the MH (Table 4).

[67] The reconstruction is also the best where the correlation between annual mean $\delta^{18}O_p$ and P is the most negative. For example, the spatial correlation between $\Delta P_{reconst}$ and ΔP_{sim} rises from 0.61 to 0.68 (Table 4) when we choose a cutoff of −0.7 compared to −0.25: where the local P is the main control on $\delta^{18}O_p$ at the interannual scale, it is also the case at the climatic scale. Consequently, changes over land are generally not well captured by the reconstruction, as expected from the lower local correlation there: $\delta^{18}O_p$ in South America, in particular, has been shown to depend more on upstream precipitation [*Vimeux et al.*, 2005].

[68] The reconstruction overestimates the magnitude of precipitation changes (Figure 16d, blue): this means that the $\delta^{18}O_p - P$ slope at the climatic scale is larger in absolute value than the annual slope used in the reconstruction, as was already pointed out for the Mid-Holocene simulation (section 3) and consistent with *Lee et al.* [2009].

[69] To test the importance of a local calibration, we reconstructed the LGM-PD ΔP for the CLIMAP simulation using the same slope at all grid points (Figure 16d, green). The slope yielding, on average, the minimum reconstruction error is −0.7‰/(mm/d), which is significantly stronger than the interannual slope (ranging from −0.3 to −0.6‰/(mm/d)). Using a local calibration compared to a constant slope does not significantly improve the reconstruction (Table 4). Since the climatic slopes are generally higher than the interannual slopes, using a constant slope of −0.7‰/(mm/d) slightly reduces the reconstruction errors (Figure 16d, green).

[70] When taking into account the thermodynamic effect of mean SST on $\delta^{18}O_p$ (0.1‰/K) and on precipitation (2%/K), the reconstructed LGM-PD ΔP is uniformly lower by 0.5 mm/d. Therefore, this thermodynamical effect explains part of the overestimate of the reconstructed LGM precipitation.

[71] So far, we have discussed reconstructions performed at the annual mean scale, i.e., neglecting the seasonal cycle, essentially because monthly $\delta^{18}O_p$ is not available from long-term records. However, the tropical precipitation experiences strong seasonal variations, so that the isotopic records at the annual-scale record preferentially the $\Delta\delta^{18}O_p$, and thus the ΔP, during the wet season. Using annual mean $\delta^{18}O_p$ values to reconstruct the annual mean ΔP thus constitutes a likely source of errors in the reconstruction. We gave an illustrative example of this source of error in section 3.4.2, showing that over West Africa the climatic slope between PD and MH was 3 times larger when calculated with annual averages than with wet season (JJAS) averages, thus leading to an overestimation of $\Delta P_{reconst}$ of a factor of 3 just by neglecting the seasonal variability. To quantify more systematically this source of error, we reconstruct monthly ΔP using simulated monthly $\Delta\delta^{18}O_p$ and the slope calculated on present-day monthly interannual anomalies (Figure 16d, brown). In this case the reconstruction is significantly improved for positive LGM-PD changes. For the LGM CLIMAP simulation, the probability that the reconstructed ΔP relative error is smaller than 50% slightly rises to 31% (compared to 29%) when considering seasonal information (Table 4). The uncertainty in the reconstruction due to the seasonality of the precipitation is the largest for the MH simulation: the probability that the reconstructed ΔP relative error is smaller than 50% rises to 31% (compared to 16%) when considering seasonal information (Table 4). This is consistent with the strong changes in precipitation seasonality for the MH, with the precipitation increase occurring mainly during the wet season in monsoon regions.

[72] To conclude, using the PD interannual $\delta^{18}O_p - P$ slope to reconstruct past precipitation changes yields good results qualitatively: the spatial patterns of ΔP are well reconstructed, especially for past climates involving large circulation changes. Where measured changes of $\delta^{18}O_p$ are high (>2‰), it is very likely that the reconstructed ΔP has the right sign (92%): this means that interannual and climatic controls on $\delta^{18}O_p$ are similar. Quantitatively however, the reconstructed errors are high and most likely above 50%. The magnitude of the reconstructed ΔP is generally overestimated. Considering the seasonal cycle of P and $\delta^{18}O_p$ both for the calibration and reconstruction would improve the reconstructions quantitatively, in particular for past climates associated with strong changes in precipitation seasonality (e.g., MH).

5. Conclusion and Perspectives

5.1. Evaluation of LMDZ-iso

[73] We present the implementation of water-stable isotopes in the LMDZ-iso GCM, and evaluate the present-day isotopic distribution simulated at different time scales: synoptic, seasonal, and interannual, as well as for past climate changes. LMDZ-iso forced by observed SSTs reproduces the annual mean and the seasonal distribution of $\delta^{18}O_p$ reasonably well, as well as its interannual variability in the tropics. Nudging the model winds by atmospheric reanalyses improves the simulation of the interannual and synoptic variability of temperature and $\delta^{18}O$ at middle latitudes.

[74] Deuterium excess is known to be a more difficult parameter to simulate [*Mathieu et al.*, 2002]. Despite some discrepancies over tropical continents, LMDZ-iso is able to correctly simulate the average d excess values as well as the zonal gradient. LMDZ-iso is not able to reproduce the observed variability of d excess in the vapor, neither at synoptic nor at interannual scales, producing near-constant values all year long and for all years in some regions.

[75] Numerous sensitivity tests were performed on both isotopic and nonisotopic parameters of the model. The precipitation composition is most sensitive to two parameters controlling kinetic effects: λ, involved in the parameterization of the supersaturation during snow formation [*Jouzel and Merlivat*, 1984], and ϕ, involved in the parameterization of the relative humidity at the droplet contact [*Bony et al.*, 2008]. These representations of kinetic effects are thus a large source of uncertainties in isotopic modeling. More measurements are certainly needed to better constrain these processes. In particular, the degree of equilibration of the rain drops with the vapor can be parametrized in many ways [e.g., *Stewart*, 1975; *Hoffmann et al.*, 1998; *Mathieu et al.*, 2002; *Lee and Fung*, 2008; *Bony et al.*, 2008] and is difficult to evaluate owing to the scarcity of isotopic measurements in the vapor. It would thus be extremely useful to have simultaneous measurements of precipitation and vapor at the same stations to evaluate the representation of isotopic processes during rain reevaporation in models. New technology [e.g., *Gupta et al.*, 2009] now facilitates measurements in the vapor and will certainly offer new evaluation possibilities.

[76] LMDZ-iso simulates LGM isotopic compositions similar to other GCMs, with relatively realistic depletions at high latitudes, but a near-constant $\delta^{18}O$ in the tropics. Like other GCMs, LMDZ-iso has difficulties simulating the lower measured d excess during the LGM over East Antarctica, though it can simulate it in Greenland and coastal Antarctica.

5.2. Interpretation of Paleoclimatic Proxies

[77] At high latitudes, on the basis of a LGM simulation with LMDZ-iso forced by the CLIMAP SST reconstruction, we show that using the present-day spatial slope to reconstruct past temperatures leads to an underestimation of a factor of 2 in Greenland but is more adequate in Antarctica, in agreement with previous studies [*Jouzel et al.*, 2000, 2003]. However, the accuracy of this reconstruction in Antarctica strongly depends on the equator-pole SST gradients of the reconstructed past climate. If the equator-pole at LGM was weaker than reconstructed by CLIMAP, then past temperature reconstructions in Antarctica would be underestimated, in agreement with *Lee et al.* [2008].

[78] In the tropics changes in $\delta^{18}O_p$ may result from global-scale changes in SSTs, and/or from regional precipitation changes associated with changes in SSTs that are not spatially uniform. We found that changes in mean tropical SSTs have relatively little impact on $\delta^{18}O_p$ (0.1‰/K) and cannot explain the large changes in $\delta^{18}O_p$ recorded in few tropical locations for the LGM. On the other hand, large changes in $\delta^{18}O_p$ are more likely related to precipitation changes associated with a reorganization of SST patterns.

[79] We thus examine the ability of $\delta^{18}O_p$ records to reconstruct past local precipitation changes in the tropics. Our analysis suggests that past local precipitation changes can be reconstructed from $\delta^{18}O_p$ records, but only in cases where the signal to noise ratio for $\delta^{18}O_p$ is the largest. The use of a $\delta^{18}O - P$ slope calibrated locally from present-day annual data seems adequate to reconstruct at least qualitatively the broad pattern and signs of precipitation changes. However, this overestimates the magnitude of precipitation changes. Considering the seasonal cycle of precipitation and $\delta^{18}O_p$ for both the calibration and reconstruction would improve the reconstruction quantitatively. Over continents however, the sensitivity of $\delta^{18}O_p$ to upstream precipitation rather than local precipitation makes reconstructions of past precipitation at the regional scale more adequate [*Vimeux et al.*, 2005]. Besides, changes in continental recycling associated with past vegetation changes, which were not taken into account in this study, may complicate the $\delta^{18}O_p$ signal over continents [*Pierrehumbert*, 1999].

5.3. Perspectives

[80] LMDZ-iso, like other GCMs, does not simulate the large isotopic depletion measured in tropical ice cores, questioning whether all processes affecting $\delta^{18}O_p$ in the tropics are well represented. Tropical ice cores are located in mountainous regions, characterized by a complex topography which can only be resolved with high-resolution modeling [*Sturm et al.*, 2005]. Part of the difficulty in simulating the ice core isotopic data at LGM could be due to the coarse resolution of GCMs (here 2.75 × 3.5°). In the future, we plan to use the stretched grid functionality of LMDZ-iso [e.g., *Krinner et al.*, 1997a] to run zoomed simulations for present day and for LGM over low-latitude mountain regions such as the Andes and Tibet, to better simulate the relationship

between isotopes and climate and explore climatic controls on low-latitude ice core isotopic composition.

[81] Air parcels supplying precipitation to ice core regions usually travel several days over continental regions (the Amazon for the Andes, India for Tibet), over which continental recycling of precipitation occurs. The proportion of precipitation recycled to the atmosphere or lost by runoff has been shown to control continental gradients in $\delta^{18}O$ [*Rozanski et al.*, 1993]. Besides, transpiration does not fractionate relatively to the soil water [*Washburn and Smith*, 1934; *Barnes and Allison*, 1988] whereas bare soil evaporation does and is thus depleted relative to the soil water [*Moreira et al.*, 1997; *Yepez et al.*, 2003; *Williams et al.*, 2004]. A decrease in the ratio of the precipitation evapotranspired back to the atmosphere and of the proportion of the evapotranspiration occurring as transpiration, associated with vegetation changes from forests to grasslands [*Clapperton*, 1993], may contribute to the measured decrease of $\delta^{18}O_p$ in the Andes during the LGM [*Pierrehumbert*, 1999]. Moreover, processes by which precipitation is recycled (transpiration or evaporation from open water or soil) are suggested to strongly affect d excess gradients over the Amazon [*Salati et al.*, 1979; *Gat and Matsui*, 1991; *Henderson-Sellers et al.*, 2004] and thus possibly the Andean ice core d excess. Despite the potentially strong impact of land surface processes on the isotopic distribution, in LMDZ-iso as in most other GCMs, we have assumed no fractionation when recycling precipitation over land, owing to the simplicity of the land surface model. Coupling atmospheric models with more sophisticated land surface models [*Aleinov and Schmidt*, 2006; *Yoshimura et al.*, 2006] would enable a more accurate representation of isotopic fractionation over land and allow us to explore the impact of vegetation changes on continental isotopic records. Water-stable isotopes are being implemented in ORCHIDEE, the land surface component of the IPSL model, and LMDZ-ORCHIDEE-iso coupled simulations will be reported in a future paper.

[82] Finally, further global evaluations of our GCM will be carried out in the future by comparing its simulations with the newly available global isotopic data measured by satellite, in particular the Troposperic Emission Spectrometer (TES) [*Worden et al.*, 2007] and Scanning Imaging Absorption Spectrometer for Atmospheric Cartography (SCIAMACHY) [*Frankenberg et al.*, 2009] data.

Appendix A: Advection of Water-Stable Isotopes

[83] Water isotopes are advected passively during the large-scale water advection. However, for numerical reasons, the advection of water isotopes can be problematic in some schemes [e.g., *Joussaume*, 1989; *Mathieu et al.*, 2002]. We present here the *Van Leer* [1977] advection scheme used in LMDZ-iso and explain the possible problem of isotopic advection and how we handle it. To simplify, we consider in the following a unidimensional advection along the x axis, with a westerly wind.

A1. Van Leer Advection Scheme

[84] The *Van Leer* [1977] scheme used in LMDZ is a finite volume advection scheme, conserving water mass. In the grid box i, m'_i, the total air mass at time $t + \Delta t$ is a function of the total air mass at time t and the air mass fluxes on the left and right border, $U_{i-1/2}$ and $U_{i+1/2}$, respectively:

$$m'_i = m_i + U_{i-1/2} - U_{i+1/2}.$$

[85] Similarly, the averaged specific humidity in grid box i at time $t + \Delta t$, q'_i, is a function of the specific humidity at time t and the water flux on the left and right border, $F_{i-1/2}$ and $F_{i+1/2}$.

$$q_i' = \frac{q_i \cdot m_i + F_{i-1/2} - F_{i+1/2}}{m'_i}.$$

[86] Water fluxes (for example, $F_{i-1/2}$) are calculated as the product of the air mass flux ($U_{i-1/2}$) and the specific humidity of the advected air ($q_{i-1/2}^{\smile}$):

$$F_{i-1/2} = U_{i-1/2} \cdot q_{i-1/2}^{\smile}.$$

[87] In the Van Leer scheme, $q_{i-1/2}^{\smile}$ is interpolated between the averaged specific humidity of the adjacent boxes, so that $q_{i-1/2}^{\smile}$ is a function of (q_i, q_{i+1}, q_{i-1}).

[88] As long as $q_{i-1/2}^{\smile}$ is intermediate between q_i and q_{i-1}, the monotony of the scheme is ensured: q'_i remains intermediate between q_i and q_{i-1} [*Van Leer*, 1977; *Hourdin*, 2005].

A2. Implementation of Water Isotopes in the Van Leer Scheme

[89] As for water, the isotopic equivalent of specific humidity, X, is advected in finite volume

$$X_i' = \frac{X_i \cdot m_i + G_{i-1/2} - G_{i+1/2}}{m'_i},$$

where $G_{i-1/2}$ and $G_{i+1/2}$ are the isotope fluxes at the left and right boundaries. The isotope mass is thus conserved during advection. The isotope flux at the left boundary, $G_{i-1/2}$, is calculated as the product $U_{i-1/2}$ and the isotopic content of the advected air $X_{i-1/2}^{\smile}$,

$$G_{i-1/2} = U_{i-1/2} \cdot X_{i-1/2}^{\smile}.$$

[90] In a purely Lagrangian framework, transport should simultaneously conserve the water, the isotopic content, and the isotopic ratio $R = X/q$: indeed, it can be shown that if X follows the same conservation equation as q of the form $\frac{\partial q}{\partial t} + u \cdot \frac{\partial q}{\partial x} = 0$, then R also follows the same conservation equation.

[91] In the Van Leer scheme, however, owing to the discretization, X and R cannot follow simultaneously the same equation as q. A choice has thus to be made regarding how to handle the transport of water isotopes.

[92] If X were to be treated exactly like water, $X_{i-1/2}^{\smile}$ should be interpolated between the adjacent grid boxes, so that $X_{i-1/2}^{\smile}$ is a function of (X_i, X_{i+1}, X_{i-1}). Then the monotony of the transport would be ensured for q and X. However, the monotony would not be ensured for R, owing to the nonlinearity of R as a function of X and q. In particular, it could happen that the isotopic ratio after advection, R'_i, becomes either larger or smaller than the ratios in

both adjacent grid boxes. Spurious variations of the isotopic ratio could thus appear.

[93] Problems arising from representing the isotopic mixing ratio exactly like the water mixing ratio are justified physically: isotopes are not transported independently from the water but inside the water.

[94] Therefore, to ensure that isotopes are not transported without water, we calculate $X_{i-1/2}^{\smile}$ as the product of the advected water content $q_{i-1/2}^{\smile}$ and the isotopic ratio of this advected water $R_{i-1/2}^{\smile}$,

$$X_{i-1/2}^{\smile} = q_{i-1/2}^{\smile} \cdot R_{i-1/2}^{\smile}.$$

[95] To ensure the monotony of the isotopic ratio, $R_{i-1/2}^{\smile}$ is interpolated between the adjacent boxes, so that $R_{i-1/2}$ is a function of (R_i, R_{i+1}, R_{i-1}).

[96] This representation of the isotopic transport ensures both the conservation of the mass of water isotopes (finite volume scheme) and the monotony of the isotopic ratio.

[97] **Acknowledgments.** We thank Masa Kageyama, Valrie Masson-Delmotte, Gerhard Krinner, and Frédéric Hourdin for useful discussions, Gilles Delaygue and Gavin Schmidt for comments on the manuscript as part of their review of Camille Risi's Ph.D. dissertation, and three anonymous reviewers for their very constructive comments. This work benefited from financial support of the LEFE project MISSTERRE.

References

Aleinov, I., and G. A. Schmidt (2006), Water isotopes in the GISS ModelE land surface scheme, *Global Planet. Change*, *51*, 108–120.

Angert, A., J.-E. Lee, and D. Yakir (2008), Seasonal variations in the isotopic composition of near-surface water vapour in the eastern Mediterranean, *Tellus, Ser. B*, *60*(4), 674–684.

Baldini, L. M., F. McDermott, A. M. Foley, and J. U. L. Baldini (2008), Spatial variability in the European winter precipitation d^{1}8O-NAO relationship: Implications for reconstructing NAO-mode climate variability in the Holocene, *Geophys. Res. Lett.*, *35*, L04709, doi:10.1029/2007GL032027.

Barnes, C., and G. Allison (1988), Tracing of water movement in the unsaturated zone using stable isotopes of hydrogen and oxygen, *J. Hydrol.*, *100*, 143–176.

Bath, A. H. (1983), Stable isotopic evidence for paleo-recharge conditions of groundwater, in *Paleoclimates and Paleowaters: A Collection of Environmental Isotope Studies*, pp. 169–186, Int. At. Energy Agency, Vienna.

Berger, A. (1978), Long-term variations of caloric solar radiation resulting from the Earth's orbital elements, *Quat. Res.*, *9*, 139–167.

Bony, S., and K. A. Emanuel (2001), A parameterization of the cloudiness associated with cumulus convection; Evaluation using TOGA COARE data, *J. Atmos. Sci.*, *58*, 3158–3183.

Bony, S., J.-L. Dufresne, H. Le Treut, J.-J. Morcrette, and C. Senior (2004), On dynamic and thermodynamic components of cloud changes, *Clim. Dyn.*, *22*, 71–86.

Bony, S., C. Risi, and F. Vimeux (2008), Influence of convective processes on the isotopic composition (δO^{18} and δD) of precipitation and water vapor in the tropics: 1. Radiative-convective equilibrium and TOGA-COARE simulations, *J. Geophys. Res.*, *113*, D19305, doi:10.1029/2008JD009942.

Boyle, E. A. (1997), Cool tropical temperatures shift the global $\delta^1$8O-T relationship: An explanation for the ice core $\delta^1$8O–borehole thermometry conflict?, *Geophys. Res. Lett.*, *24*(3), 273–276.

Braconnot, P., et al. (2007), Results of PMIP2 coupled simulations of the Mid-Holocene and Last Glacial Maximum - Part 1: Experiments and large-scale features, *Clim. Past*, *3*, 261–277.

Bradley, R. S., M. Vuille, D. Hardy, and L. G. Thompson (2003), Low latitude ice cores record Pacific sea surface temperatures, *Geophys. Res. Lett.*, *30*(4), 1174, doi:10.1029/2002GL016546.

Cess, R. D., and G. L. Potter (1988), A methodology for understanding and intercomparing atmospheric climate feedback processes in general circulation models, *J. Geophys. Res.*, *93*(D7), 8305–8314.

Ciais, P., and J. Jouzel (1994), Deuterium and oxygen 18 in precipitation: Isotopic model, including cloud processes, *J. Geophys. Res.*, *99*(D8), 16,793–16,803.

Ciais, P., W. White, J. Jouzel, and J. Petit (1995), The origin of present-day Antarctic precipitation from surface snow deuterium excess data, *J. Geophys. Res.*, *100*(D9), 18,917–18,927.

Clapperton, C. M. (1993), Nature of environmental changes in South America at the Last Glacial Maximum, *Palaeogeogr. Palaeoclimatol. Palaeoecol.*, *101*, 189–208.

CLIMAP Project Members (1981), Seasonal reconstructions of the Earth's surface at the Last Glacial Maximum, *Tech. Rep. GM-36*, Geol. Soc. Am., Boulder, Colo.

Coplen, T. (1988), Normalization of oxygen and hydrogen isotope data, *Chem. Geol.*, *72*, 293–297.

Cruz, F. W., S. J. Burns, I. Karmann, W. D. Sharp, M. Vuille, A. O. Cardoso, J. A. Ferrari, P. L. S. Dias, and O. J. Viana (2005a), Insolation-driven changes in atmospheric circulation over the past 116,000 years in subtropical Brazil, *Nature*, *434*, 63–66.

Cruz, F. W., I. Karmann, O. Viana Jr., J. A. Burns, M. Ferrari, M. Vuille, A. N. Sial, and M. Z. Moreira (2005b), Stable isotope study of cave percolation waters in subtropical Brazil: Implications for paleoclimate inferences from speleothems, *Chem. Geol.*, *220*, 245–262.

Cruz, F. W., S. J. Burns, I. Karmann, W. Sharp, and M. Vuille (2006), Reconstruction of regional atmospheric circulation features during the late Pleistocene in subtropical Brazil from oxygen isotope composition of speleothems, *Earth Planet. Sci. Lett.*, *248*(1–2), 495–507, doi:10.1016/j.epsl.2006.06.019.

Cruz, F. W., et al. (2009), Orbitally driven east-west antiphasing of South American precipitation, *Nat. Geosci.*, *2*, 210–214.

Dansgaard, W. (1953), The abundance of ^{1}8O in atmospheric water and water vapour, *Tellus*, *5*, 461–469.

Dansgaard, W. (1964), Stable isotopes in precipitation, *Tellus*, *16*, 436–468.

Delmotte, M., V. Masson, J. Jouzel, and V. Morgan (2000), A seasonal deuterium excess signal at Law Dome, coastal eastern Antarctica: A Southern Ocean signature, *J. Geophys. Res.*, *105*(D6), 7187–7197.

Ducoudré, N., K. Laval, and A. Perrier (1993), SECHIBA, a new set of parametrizations of the hydrological exchanges at the land-atmosphere interface within the LMD atmospheric general circulation model, *J. Clim.*, *6*, 248–273.

Ekaykin, A. A., and V. Y. Lipenkov (2008), Formation of the ice core isotope composition, paper presented at 2nd International Workshop on Physics of Ice Core Records (PICR-2), Hokkaido Univ., Sapporo, Japan.

Emanuel, K. A. (1991), A scheme for representing cumulus convection in large-scale models, *J. Atmos. Sci.*, *48*, 2313–2329.

Farrera, I., et al. (1999), Tropical climates at the Last Glacial Maximum: A new synthesis of terrestrial palaeoclimate data. I. Vegetation, lake-levels and geochemistry, *Clim. Dyn.*, *15*, 823–856.

Frankenberg, C., et al. (2009), Dynamic processes governing lower-tropospheric HDO/H_2O ratios as observed from space and ground, *Science*, *325*, 1374–1377.

Fritz, S., et al. (2003), Hydrologic variation during the last 170,000 years in the Southern Hemisphere tropics of South America, *Quat. Res.*, *61*, 95–104.

Fujita, K., and O. Abe (2006), Stable isotopes in daily precipitation at Dome Fuji, East Antarctica, *Geophys. Res. Lett.*, *33*, L18503, doi:10.1029/2006GL026936.

Gasse, F. (2000), Hydrological changes in the African tropics since the Last Glacial Maximum, *Quat. Sci. Rev.*, *19*, 189–211.

Gat, J. R., and E. Matsui (1991), Atmospheric water balance in the Amazon basin: An isotopic evapotranspiration model, *J. Geophys. Res.*, *96*(D7), 13,179–13,188.

Gates, W. L. (1992), AMIP: The Atmospheric Model Intercomparison Project, *Bull. Am. Meteorol. Soc.*, *73*, 1962–1970.

Grandpeix, J. Y., V. Phillips, and R. Tailleux (2004), Improved mixing representation in Emanuel's convection scheme, *Q. J. R. Meteorol. Soc.*, *130*, 3207–3222.

GRIP Members (1993), Climate instability during the last interglacial period recorded in the GRIP ice core, *Nature*, *364*, 203–207.

Grootes, P. M., E. J. Steig, M. Stuiver, E. D. Waddington, and D. L. Morse (2001), The Taylor Dome Antarctic ^{1}8O record and globally synchronous change in climate, *Quat. Res.*, *56*, 289–298.

Gupta, P., D. Noone, J. Galewsky, C. Sweeney, and B. H. Vaughn (2009), Demonstration of high-precision continuous measurements of water vapor isotopologues in laboratory and remote field deployments using wavelength-scanned cavity ring-down spectroscopy (WS-CRDS) technology, *Rapid Commun. Mass Spectrom.*, *23*, 2534–2542.

Held, I. M., and B. J. Soden (2006), Robust responses of the hydrological cycle to global warming, *J. Clim.*, *19*, 5686–5699.

Held, I. M., T. L. Delworth, K. L. Findell, and T. R. Knutson (2005), Simulation of Sahel drought in the 20th and 21st centuries, *Proc. Natl. Acad. Sci., U. S. A.*, *102*, 17,891–17,896, doi:10.1073/pnas.0509057,102.

Henderson-Sellers, A., K. McGuffie, and H. Zhang (2001), Stable isotopes as validation tools for global climate model predictions of the impact of Amazonian deforestation, *J. Clim*, *15*, 2664–2677.

Henderson-Sellers, A., K. McGuffie, D. Noone, and P. Irannejad (2004), Using stable water isotopes to evaluate basin-scale simulations of surface water budgets, *J. Hydrometeorol.*, *5*, 805–822.

Hoffmann, G. (2003), Taking the pulse of the tropical water cycle, *Science*, *301*, 776–777.

Hoffmann, G., M. Werner, and M. Heimann (1998), Water isotope module of the ECHAM atmospheric general circulation model: A study on timescales from days to several years, *J. Geophys. Res.*, *103*(D14), 16,871–16,896.

Hoffmann, G., et al. (2003), Coherent isotope history of Andean ice cores over the last century, *Geophys. Res. Lett.*, *30*(4), 1179, doi:10.1029/2002GL014870.

Hourdin, F. (2005), Représentation du transport direct et inverse dans les modèles globaux de climat et étude des couplages entre composition et dynamique atmosphérique sur Titan, Habilitation à Diriger des Rech., Orsay, France.

Hourdin, F., et al. (2006), The LMDZ4 general circulation model: Climate performance and sensitivity to parametrized physics with emphasis on tropical convection, *Clim. Dyn.*, *27*, 787–813.

Huffman, G. J., P. Arkin, and J. Janowiak (1997), The Global Precipitation Climatology Project (GPCP) combined precipitation dataset, *Bull. Am. Meteorol. Soc.*, *78*, 5–20.

Johnsen, S., W. Dansgaard, H. Clausen, and J. C. Langway (1972), Oxygen isotope profiles through the Antarctic and Greenland ice sheets, *Nature*, *235*, 429–434.

Johnsen, S., W. Dansgaard, and J. White (1989), Origin of Arctic precipitation under present and glacial conditions, *Tellus, Ser. B*, *41*, 452–458.

Johnsen, S., H. Clausen, W. Dansgaard, N. Gundestrup, M. Hansson, P. Jonsson, J. Steffensen, and A. Sveinbjörnsdottir (1992), A "deep" ice core from East Greenland, *Medd. Groenl. Geosci.*, *29*, 1–22.

Joussaume, S. (1989), Simulations du climat du dernier maximum glaciaire à l'aide d'un modèle de circulation générale de l'atmosphère incluant une modélisation du cycle des isotopes de l'eau et des poussières d'origine désertique, Ph.D. thesis, Univ. Marie et Pierre Curie, Paris.

Joussaume, S., and J. Jouzel (1993), Paleoclimatic tracers: An investigation using an atmospheric general circulation model under ice age conditions: 2. Water isotopes, *J. Geophys. Res.*, *98*(D2), 2807–2830.

Joussaume, S., and K. E. Taylor (1995), Status of the paleoclimate modeling intercomparison project, in *Proceedings of the First International AMIP Scientific Conference*, edited by W. L. Gates, pp. 425–430, World Meteorol. Org., Geneva.

Joussaume, S., J. Jouzel, and R. Sadourny (1984), A general circulation model of water isotope cycles in the atmosphere, *Nature*, *311*, 24–29.

Joussaume, S., et al. (1999), Monsoon changes for 6000 years ago: Results of 18 simulations from the Paleoclimate Modeling Intercomparison Project (PMIP), *Geophys. Res. Lett.*, *26*(7), 859–862.

Jouzel, J. (1999), Calibrating the isotopic paleothermometer, *Science*, *286*, 910–911.

Jouzel, J. (2003), Water stable isotopes: Atmospheric composition and applications in polar ice core studies, *Treatise Geochem.*, *4*, 213–243.

Jouzel, J., and L. Merlivat (1984), Deuterium and oxygen 18 in precipitation: Modeling of the isotopic effects during snow formation, *J. Geophys. Res.*, *89*(D7), 11,749–11,757.

Jouzel, J., R. D. Koster, R. J. Suozzo, G. L. Russel, J. W. C. White, and W. S. Broecker (1987), Simulations of the HDO and $H_2^{18}O$ atmospheric cycles using the NASA GISS General Circulation Model: The seasonal cycle for present-day conditions, *J. Geophys. Res.*, *92*(D12), 14,739–14,760.

Jouzel, J., R. Koster, R. Suozzo, and G. L. Russel (1994), Stable water isotope behavior during the Last Glacial Maximum: A general circulation model analysis, *J. Geophys. Res.*, *99*(D12), 25,791–25,801.

Jouzel, J., G. Hoffmann, R. D. Koster, and V. Masson (2000), Water isotopes in precipitation: Data/model comparison for present-day and past climates, *Quat. Sci. Rev.*, *19*, 363–379.

Jouzel, J., F. Vimeux, N. Caillon, G. Delaygue, G. Hoffmann, V. Masson-Delmotte, and F. Parrenin (2003), Magnitude of isotope/temperature scaling for interpretation of central Antarctic ice cores, *J. Geophys. Res.*, *108*(D12), 4361, doi:10.1029/2002JD002677.

Kalnay, E., et al. (1996), The NCEP/NCAR 40-year reanalysis project, *Bull. Am. Meteorol. Soc.*, *77*, 437–470.

Krinner, G., and M. Werner (2003), Impact of precipitation seasonality changes on isotopic signals in polar ice cores: A multi-model analysis, *Earth Planet. Sci. Lett.*, *216*, 525–538.

Krinner, G., C. Genthon, Z.-X. Li, and P. L. Van (1997a), Studies of the Antarctic climate with a stretched-grid general circulation model, *J. Geophys. Res*, *102*(D12), 13,731–13,745.

Krinner, G., C. Genton, and J. Jouzel (1997b), GCM analysis of local influences on ice core delta signals, *Geophys. Res. Lett*, *24*(22), 2825–2828.

Krinner, G., N. Viovy, N. de Noblet-Ducoudré, J. Ogee, J. Polcher, P. Friedlingstein, P. Ciais, S. Sitch, and I. C. Prentice (2005), A dynamic global vegetation model for studies of the coupled atmosphere-biosphere system, *Global Biogeochem. Cycles*, *19*, GB1015, doi:10.1029/2003GB002199.

Kutzbach, J. E., X. Liu, Z. Liu, and G. Chen (2008), Simulation of the evolutionary response of global summer monsoons to orbital forcing over the past 280,000 years, *Clim. Dyn.*, *30*, 567–579, doi:10.1007/s00382-007-0308-z.

Labeyrie, L. D., J. C. Duplessy, and P. L. Blanc (1987), Variations in mode of formation and temperature of oceanic deep waters over the past 125,000 years, *Nature*, *327*, 477–482.

Landais, A., E. Barkan, and B. Luz (2008), Record of $\delta^{18}O$ and ^{17}O-excess in ice from Vostok Antarctica during the last 150,000 years, *Geophys. Res. Lett.*, *35*, L02709, doi:10.1029/2007GL032096.

Lawrence, J. R., S. D. Gedzelman, D. Dexheimer, H.-K. Cho, G. D. Carrie, R. Gasparini, C. R. Anderson, K. P. Bowman, and M. I. Biggerstaff (2004), Stable isotopic composition of water vapor in the tropics, *J. Geophys. Res.*, *109*, D06115, doi:10.1029/2003JD004046.

Lee, J.-E., and I. Fung (2008), "Amount effect" of water isotopes and quantitative analysis of post-condensation processes, *Hydrol. Processes*, *22*(1), 1–8.

Lee, J.-E., I. Fung, D. DePaolo, and C. C. Fennig (2007), Analysis of the global distribution of water isotopes using the NCAR atmospheric general circulation model, *J. Geophys. Res.*, *112*, D16306, doi:10.1029/2006JD007657.

Lee, J.-E., I. Fung, D. J. DePaolo, and B. Otto-Bliesner (2008), Water isotopes during the Last Glacial Maximum: New general circulation model calculations, *J. Geophys. Res.*, *113*, D19109, doi:10.1029/2008JD009859.

Lee, J.-E., K. Johnson, and I. Fung (2009), Precipitation over South America during the Last Glacial Maximum: An analysis of the "amount effect" with a water isotop-enabled general circulation model, *Geophys. Res. Lett.*, *36*, L19701, doi:10.1029/2009GL039265.

Liu, C., and E. J. Zipser (2005), Global distribution of convection penetrating the tropical tropopause, *J. Geophys. Res.*, *110*, D23104, doi:10.1029/2005JD006063.

Lorius, C., L. Merlivat, J. Jouzel, and M. Pourchet (1979), A 30,000 yr isotope climatic record from Antarctic ice, *Nature*, *280*, 644–648.

Lorius, C., J. Jouzel, C. Ritz, L. Merlivat, N. I. Barkov, Y. S. Korotkevitch, and V. M. Kotlyakov (1985), A 150,000-year climate record from Antarctic ice, *Nature*, *316*, 591–596.

Majoube, M. (1971a), Fractionnement en O^18 entre la glace et la vapeur d'eau, *J. Chim. Phys. Phys. Chim. Biol.*, *68*, 625–636.

Majoube, M. (1971b), Fractionnement en Oxygène 18 et en Deutérium entre l'eau et sa vapeur, *J. Chim. Phys. Phys. Chim. Biol.*, *10*, 1423–1436.

MARGO Project Members (2009), Constraints on the magnitude and patterns of ocean cooling at the Last Glacial Maximum, *Nat. Geosci.*, *2*, 127–132.

Marti, O., et al. (2005), The new IPSL climate system model: IPSL-CM4, *Tech. Rep. 26*, IPSL, Paris.

Masson-Delmotte, V., J. Jouzel, A. Landais, M. Stievenard, S. J. Johnsen, J. W. C. White, M. Werner, A. Sveinbjornsdottir, and K. Fuhrer (2005a), GRIP Deuterium excess reveals rapid and orbital-scale changes in Greenland moisture origin, *Science*, *309*, 118–121.

Masson-Delmotte, V., et al. (2005b), Holocene climatic changes in Greenland: Different deuterium excess signals at Greenland Ice Core Project (GRIP) and NorthGRIP, *J. Geophys. Res.*, *110*, D14102, doi:10.1029/2004JD005575.

Masson-Delmotte, V., et al. (2006), Past and future polar amplification of climate change: Climate model intercomparisons and ice-core constraints, *Clim. Dyn.*, *26*, 513–529.

Masson-Delmotte, V., et al. (2008), A review of Antarctic surface snow isotopic composition: Observations, atmospheric circulation and isotopic modelling, *J. Clim.*, *21*, 3359–3387.

Mathieu, R., D. Pollard, J. Cole, J. W. C. White, R. S. Webb, and S. L. Thompson (2002), Simulation of stable water isotope variations by the GENESIS GCM for modern conditions, *J. Geophys. Res.*, *107*(D4), 4037, doi:10.1029/2001JD900255.

Meehl, G. A., K. Covey, T. Delworth, M. Latif, B. McAvaney, J. F. B. Mitchell, R. J. Stouffer, and K. Taylor (2007), The WCRP CMIP3 multimodel dataset: A new era in climate change research, *Bull. Am. Meteorol. Soc.*, *7*, 1383–1394.

Merlivat, L., and J. Jouzel (1979), Global climatic interpretation of the deuterium-oxygen 18 relationship for precipitation, *J. Geophys. Res.*, *84*(C8), 5029–5332.

Merlivat, L., and G. Nief (1967), Fractionnement isotopique lors des changements d'états solide-vapeur et liquide-vapeur de l'eau à des températures inférieures à 0C, *Tellus*, *19*, 122–127.

Moreira, M., L. Sternberg, L. Martinelli, R. Victoria, E. Barbosa, C. Bonates, and D. Nepstad (1997), Contribution of transpiration to forest ambient vapor based on isotopic measurements, *Global Change Biol.*, *3*, 439–450.

Nesbitt, S. W., and E. J. Zipser (2003), The diurnal cycle of rainfall and convective intensity according to three years of TRMM measurements, *J. Clim.*, *16*, 1456–1475.

NGRIP Members (2004), High-resolution record of Northern Hemisphere climate extending into the last interglacial period, *Nature*, *431*, 147–151.

Noone, D. (2008), The influence of midlatitude and tropical overturning circulation on the isotopic composition of atmospheric water vapor and Antarctic precipitation, *J. Geophys. Res.*, *113*, D04102, doi:10.1029/2007JD008892.

Noone, D., and I. Simmonds (2002a), Associations between δ^{18}O of water and climate parameters in a simulation of atmospheric circulation for 1979–95, *J. Clim.*, *15*, 3150–3169.

Noone, D., and I. Simmonds (2002b), Annular variations in moisture transport mechanisms and the abundance of δ^{18}O in Antarctic snow, *J. Geophys. Res.*, *107*(D24), 4742, doi:10.1029/2002JD002262.

Peltier, W. R. (1994), Ice age paleotopography, *Science*, *265*, 195–201.

Pierrehumbert, R. T. (1999), Huascaran δ^{18}O as an indicator of tropical climate during the Last Glacial Maximum, *Geophys. Res. Lett.*, *26*(9), 1345–1348.

Pinot, S., G. Ramstein, S. P. Harrison, I. C. Prentice, J. Guiot, M. Stute, and S. Joussaume (1999), Tropical paleoclimates at the Last Glacial Maximum: Comparison of Paleoclimate Modeling Intercomparison Project (PMIP) simulations and paleodata, *Clim. Dyn.*, *15*, 857–874.

Ramirez, E., et al. (2003), A new Andean deep ice core from Nevado Illimani (6350 m), Bolivia, *Earth Planet. Sci. Lett.*, *212*, 337–350.

Risi, C., S. Bony, and F. Vimeux (2008a), Influence of convective processes on the isotopic composition (δ^{18}O and δD) of precipitation and water vapor in the tropics: 2. Physical interpretation of the amount effect, *J. Geophys. Res.*, *113*, D19306, doi:10.1029/2008JD009943.

Risi, C., S. Bony, F. Vimeux, L. Descroix, B. Ibrahim, E. Lebreton, I. Mamadou, and B. Sultan (2008b), What controls the isotopic composition of the African monsoon precipitation? Insights from event-based precipitation collected during the 2006 AMMA campaign, *Geophys. Res. Lett.*, *35*, L24808, doi:10.1029/2008GL035920.

Rosnay, P. D., and J. Polcher (1998), Modelling root water uptake in a complex land surface scheme coupled to a GCM, *Hydrol. Earth Sci.*, *2*, 239–255.

Rozanski, K., L. Araguas-Araguas, and R. Gonfiantini (1993), Isotopic patterns in modern global precipitation, in *Climate Change in Continental Isotopic Records*, *Geophys. Monogr. Ser.*, vol. 78, edited by P. K. Swart, pp. 1–36, AGU, Washington, D. C.

Salati, E., A. Dall'Olio, E. Matsui, and J. Gat (1979), Recycling of water in the Amazon basin: An isotopic study, *Water Resour. Res.*, *15*, 1250–1258.

Schmidt, G., G. Hoffmann, D. Shindell, and Y. Hu (2005), Modelling atmospheric stable water isotopes and the potential for constraining cloud processes and stratosphere-troposphere water exchange, *J. Geophys. Res.*, *110*, D21314, doi:10.1029/2005JD005790.

Schmidt, G., A. LeGrande, and G. Hoffmann (2007), Water isotope expressions of intrinsic and forced variability in a coupled ocean-atmosphere model, *J. Geophys. Res.*, *112*, D10103, doi:10.1029/2006JD007781.

Smith, J. A., G. O. Seltzer, D. L. Farber, D. T. Rodbell, and R. C. Finkel (2005), Early local Last Glacial Maximum in the tropical Andes, *Science*, *308*, 678–681.

Sodemann, H., V. Masson-Delmotte, C. Schwierz, B. M. Vinther, and H. Wernli (2008), Interannual variability of Greenland winter precipitation sources: 2. Effects of North Atlantic Oscillation variability on stable isotopes in precipitation, *J. Geophys. Res.*, *113*, D12111, doi:10.1029/2007JD009416.

Stenni, B., V. Masson-Delmotte, S. Johnsen, J. Jouzel, A. Longinelli, E. Monnin, R. Rthlisberger, and E. Selmo (2001), An oceanic cold reversal during the last deglaciation, *Science*, *293*, 2074–2077.

Stewart, M. K. (1975), Stable isotope fractionation due to evaporation and isotopic exchange of falling waterdrops: Applications to atmospheric processes and evaporation of lakes, *J. Geophys. Res.*, *80*(9), 1133–1146.

Sturm, C., F. Vimeux, and H. Krinner (2007), Intraseasonal variability in South America recorded in stable water isotopes, *J. Geophys. Res.*, *112*, D20118, doi:10.1029/2006JD008298.

Sturm, K. (2005), Regional atmospheric modelling of the stable water isotope cycle, Ph.D. thesis, Univ. Joseph Fourier, Grenoble, France.

Sturm, K., G. Hoffmann, B. Langmann, and W. Stichler (2005), Simulation of δ^{18}O in precipitation by the regional circulation model REMO$_{iso}$, *Hydrol. Processes*, *19*, 3425–3444.

Stute, M., and S. Talma (1998), Glacial temperature and moisture transport regimes reconstructed from noble gas and δ^{18}O, Stampriet aquifer, Namibia, in *Isotope Techniques in the Study of Past and Current Environmental Changes in the Hydrosphere and the Atmosphere: Proceedings of Vienna Symposium 1997*, *SM-349/53*, pp. 307–328, IAEA, Vienna.

Sylvestre, F. (2009), Moisture pattern during the Last Glacial Maximum in South America, in *Past Climate Variability in South America and Surrounding Regions*, *Dev. Paleoenviron. Res.*, vol. 14, edited by F. Vimeux et al., pp. 3–27, Springer, New York.

Thompson, L., L. Mosley-Thompson, M. Davis, J. Bolzan, T. Yao, N. Gundestrup, X. Wu, L. Klein, and Z. Xie (1989), Holocene-late Pleistocene climatic ice core records from Quinghai-Tibetan Plateau, *Science*, *246*, 474–477.

Thompson, L. G., E. Mosley-Thompson, M. E. Davis, P.-N. Lin, K. A. Henderson, J. Cole-Dai, J. F. Bolzan, and K. B. Liu (1995), Late glacial stage and Holocene tropical ice core records from Huascaràn, Peru, *Science*, *269*, 46–50, doi:10.1126/science.269.5220.46.

Thompson, L., et al. (1997), Tropical climate instability: The last glacial cycle from a Qinghai-Tibetan ice core, *Science*, *276*, 1821–1825.

Thompson, L. G., et al. (1998), A 25,000-year tropical climate history from Bolivian ice cores, *Science*, *282*, 1858–1864.

Thompson, L. G., E. Mosley-Thompson, and K. A. Henderson (2000), Ice-core paleoclimate records in tropical South America since the Last Glacial Maximum, *J. Quat. Sci.*, *15*, 1579–1600.

Tindall, J. C., P. Valdes, and L. C. Sime (2009), Stable water isotopes in HadCM3: Isotopic signature of El Niño–Southern Oscillation and the tropical amount effect, *J. Geophys. Res.*, *114*, D04111, doi:10.1029/2008JD010825.

Uemura, R., Y. Matsui, K. Yoshimura, H. Motoyama, and N. Yoshida (2008), Evidence of deuterium-excess in water vapour as an indicator of ocean surface conditions, *J. Geophys. Res.*, *113*, D19114, doi:10.1029/2008JD010209.

Uppala, S., et al. (2005), The ERA-40 re-analysis, *Q. J. R. Meteorol. Soc.*, *131*, 2961–3012.

Vaikmae, R., J. Jouzel, J. R. Petit, and M. Stievenard (1993), A new Antarctic climate record from Dome B ice core, paper presented at Isotopic Technique in the Study of Past and Current Environmental Changes in the Hydrosphere and Atmosphere, Int. At. Energy Agency, Vienna.

van Breukelen, M., H. Vonhof, J. Hellstrom, W. Wester, and D. Kroon (2008), Fossil dripwater in stalagmites reveals Holocene temperature and rainfall variation in Amazonia, *Earth Planet. Sci. Lett.*, *275*(1–2), 54–60.

Van Leer, B. (1977), Towards the ultimate conservative difference scheme: IV. A new approach to numerical convection, *J. Comput. Phys.*, *23*, 276–299.

van Ommen, T. D., and T. Morgan (1997), Calibrating the ice core paleothermometer using seasonality, *J. Geophys. Res.*, *102*(D8), 9351–9357.

Vimeux, F., V. Masson, G. Delaygue, J. Jouzel, J. R. Petit, and M. Stievenard (2001), A 420,000 year deuterium excess record from East Antarctica: Information on past changes in the origin of precipitation at Vostok, *J. Geophys. Res.*, *106*(D23), 31,863–31,873.

Vimeux, F., R. Gallaire, S. Bony, G. Hoffmann, and J. C. H. Chiang (2005), What are the climate controls on δD in precipitation in the Zongo Valley (Bolivia)? Implications for the Illimani ice core interpretation, *Earth Planet. Sci. Lett.*, *240*, 205–220.

Vimeux, F., P. Ginot, M. Schwikowski, M. Vuille, G. Hoffmann, L. G. Thompson, and U. Schotterer (2009), Climate variability during the last 1000 years inferred from Andean ice cores: A review of methodology and recent results, *Palaeogeogr. Palaeoclimatol. Palaeoecol.*, *281*, 229–241, doi:10.1016/j.palaeo.2008.03.054.

Vuille, M., and M. Werner (2005), Stable isotopes in precipitation recording South American summer monsoon and ENSO variability: observations and model results, *Clim. Dyn.*, *25*, 401–413.

Vuille, M., R. S. Bradley, M. Werner, R. Healy, and F. Keimig (2003), Modeling δ^{18}O in precipitation over the tropical Americas: 1. Interannual variability and climatic controls, *J. Geophys. Res.*, *108*(D6), 4174, doi:10.1029/2001JD002038.

Wang, X., A. S. Auler, R. L. Edwards, H. Cheng, E. Ito, and M. Solheid (2006), Interhemispheric anti-phasing of rainfall during the last glacial period, *Quat. Sci. Rev.*, *25*, 3391–3403.

Wang, Y., et al. (2008), Millennial- and orbital-scale changes in the East Asian monsoon over the past 224,000 years, *Nature*, *451*, 1090–1093.

Washburn, E., and E. Smith (1934), The isotopie fractionation of water by physiological processes, *Science*, *79*, 188–189.

Werner, M., U. Mikolajewicz, M. Heimann, and G. Hoffmann (2000), Borehole versus isotope temperatures on Greenland: Seasonality does matter, *Geophys. Res. Lett.*, *27*(5), 723–726.

Werner, M., M. Heimann, and G. Hoffmann (2001), Isotopic composition and origin of polar precipitation in present and glacial climate simulations, *Tellus, Ser. B*, *53*, 53–71.

White, J. W. C., L. K. Barlow, D. Fisher, P. Grootes, J. Jouzel, S. J. Johnsen, M. Stuiver, and H. Clausen (1997), The climate signal in the stable isotopes of snow from Summit, Greenland: Results of comparisons with modern climate observations, *J. Geophys. Res.*, *102*(C12), 26,425–26,439.

Williams, D. G., et al. (2004), Evapotranspiration components determined by stable isotope, sap flow and eddy covariance techniques, *Agric. For. Meteorol.*, *125*, 241–258.

Worden, J., D. Noone, and K. Bowman (2007), Importance of rain evaporation and continental convection in the tropical water cycle, *Nature*, *445*, 528–532.

Yepez, E., S. Williams, R. Scott, and G. Lin (2003), Partitioning overstory and understory evapotranspiration in a semiarid savanna woodland from the isotopic composition of water vapor, *Agric. For. Meteorol.*, *119*, 53–68.

Yoshimura, K., T. Oki, N. Ohte, and S. Kanae (2003), A quantitative analysis of short-term ^{18}O variability with a Rayleigh-type isotope circulation model, *J. Geophys. Res.*, *108*(D20), 4647, doi:10.1029/2003JD003477.

Yoshimura, K., S. Miyazaki, S. Kanae, and T. Oki (2006), Iso-MATSIRO, a land surface model that incorporates stable water isotopes, *Global Planet. Change*, *51*, 90–107.

Yoshimura, K., M. Kanamitsu, D. Noone, and T. Oki (2008), Historical isotope simulation using reanalysis atmospheric data, *J. Geophys. Res.*, *113*, D19108, doi:10.1029/2008JD010074.

S. Bony and C. Risi, LMD, IPSL, UPMC, CNRS, 4, Place Jussieu, F-75005 Paris, France. (crlmd@lmd.jussieu.fr)

J. Jouzel, LSCE, IPSL (CEA, CNRS, UVSQ), Bt 701, Orme des Merisiers, F-91191 Gif-sur-Yvette, France.

F. Vimeux, UR Great Ice, IRD, LSCE, IPSL (CEA, CNRS, UVSQ), Bt 701, Orme des Merisiers, F-91191 Gif-sur-Yvette, France.